nature geoscience

SUPPLEMENTARY INFORMATION

DOI: 10.1038/NGEO1955

Three decades of global methane sources and sinks

Stefanie Kirschke[1], Philippe Bousquet[1], Philippe Ciais[1], Marielle Saunois[1], Josep G. Canadell[2], Edward J. Dlugokencky[3], Peter Bergamaschi[4], Daniel Bergmann[5], Donald R. Blake[6], Lori Bruhwiler[3], Philip Cameron-Smith[5], Simona Castaldi[7,8], Frédéric Chevallier[1], Liang Feng[9], Annemarie Fraser[9], Paul J. Fraser[15], Martin Heimann[10], Elke L. Hodson[11], Sander Houweling[12,13], Béatrice Josse[14], Paul B. Krummel[15], Jean-François Lamarque[16], Ray L. Langenfelds[15], Corinne Le Quéré[17], Vaishali Naik[18], Simon O'Doherty[19], Paul I. Palmer[9], Isabelle Pison[1], David Plummer[20], Benjamin Poulter[1], Ronald G. Prinn[21], Matt Rigby[22], Bruno Ringeval[13,23,24], Monia Santini[8], Martina Schmidt[1], Drew T. Shindell[25], Isobel J. Simpson[6], Renato Spahni[26], L. Paul Steele[15], Sarah A. Strode[27,28], Kengo Sudo[29], Sophie Szopa[1], Guido R. van der Werf[30], Apostolos Voulgarakis[25,31], Michiel van Weele[32], Ray F. Weiss[33], Jason E. Williams[32], Guang Zeng[34]

[1]LSCE-CEA-UVSQ-CNRS France, [2]Global Carbon Project, CSIRO Marine and Atmospheric Research, Australia, [3]NOAA ESRL, USA [3]Institute for Environment and Sustainability, [4]Joint Research Centre, Italy, [5]Lawrence Livermore National Laboratory, USA, [6]University of California Irvine, USA, [7]Department of Environmental Sciences, Second University of Naples, Italy, [8]Centro euro-Mediterraneo per i Cambiamenti Climatici CMCC, Lecce, Italy, [9]School of Geosciences, University of Edinburgh, UK, [10]MPI Biogeochemistry, Germany, [11]Swiss Federal Research Institute WSL, Switzerland, [12]SRON, Netherlands institute for space research, The Netherlands, [13]Institue for Marine and Atmospheric research Utrecht, The Netherlands, [14]Météo France, France, [15]Centre for Australian Weather and Climate Research/CSIRO Marine and Atmospheric Research, Aspendale, Victoria, Australia, [16]NCAR, USA, [17]Tyndall Centre for Climate Change Research, UK, [18]UCAR/GFDL, USA, [19]University of Bristol, UK, [20]CCCma, Environment Canada, [21]Massachusetts Institute of Technology, USA, [22]School of Chemistry, University of Bristol, Bristol, UK, [23]IMAU,

Utrecht University, The Netherlands, [24]Department of Systems Ecology, VU University Amsterdam, The Netherlands, [25]NASA GISS, USA, [26]University of Bern, Switzerland, [27]NASA GSFC, USA, [28]Universities Space Research Association, USA, [29]Graduate School of Environmental Studies, Nagoya University Furo-cho, Japan, [30]VU University, The Netherlands, [31]Department of Physics, Imperial College, London, UK, [32]Royal Netherlands Meteorological Institute (KNMI), The Netherlands, [33]Scripps Institution of Oceanography, USA [34]National Institute of Water and Atmospheric Research, New Zealand.

Corresponding author: Philippe Bousquet, philippe.bousquet@lsce.ipsl.fr

I Supporting text, figures, and tables

I.1 Supporting text

ST1 - Atmospheric CH_4 observations and growth rates for the different atmospheric networks (Figure 1).

Several types of measurements exist for atmospheric methane. High precision measurements (±3 ppb), traceable to the World Meteorological Organisation (WMO) mole fraction international calibration scale, are available from 160 fixed surface stations[1-4] and more than 30 mobile stations (ships and aircraft)[5,6,7]. Atmospheric observations consist of both flask samples (grab samples, weekly or bi-weekly) and continuous data (hourly or better resolution). Precise measurements of total column CH_4 mixing ratio (XCH_4) are provided from the Total Column Carbon Observing Network (TCCON) of 25 ground based remote-sensing stations which are only indirectly linked to the WMO scale[8,9]. Isotopic measurements (^{13}C-CH_4 and deuterium-methane, CH_3D) are performed at a subset of surface stations and help separate biogenic from other CH_4 sources[10-15]. Measurements of ^{14}C-CH_4 at one station help quantify the contribution of fossil CH_4 to the total source mix[16]. Finally, space-borne XCH_4 retrievals (over the last decade only) predominantly originate from three satellites[17-21] providing global coverage albeit with much lower precision (e.g. random error of ~30 ppb for SCIAMACHY[22] and latitudinal biases of up to 40 ppb[23]).

Figure 1 of the paper plots the atmospheric globally averaged CH_4 mole fractions and the associated growth rates for the four global trace gas atmospheric monitoring networks with a global coverage NOAA/ESRL[24], AGAGE[25], CSIRO[26] and UCI[27]. For NOAA/ESRL, AGAGE AND CSIRO. The growth rates have been calculated as the derivative of a trend curve computed according to Thoning et al., (1989)[28]. The growth rate calculations for the UCI network are described further below. Decadal global means of CH_4 mole fractions for the 1990s (1746 ppb) and the 2000s (1776 ppb) are remarkably consistent between the four networks, with respective ranges of [1743-1747 ppb] and [1775-1779 ppb]. Differences on the decadal means are mostly due to representativeness and sampling differences between networks, and to a lesser extent to instrumental errors. Indeed, regular inter-comparison between networks at various sites shows differences smaller than ±2 ppb. The decadal mean for the 1980s is more uncertain [1663-1690 ppb], possibly because of a more limited spatial and temporal coverage of some of the networks at that time. Growth rates are also very similar in the 1980s [11.3-12.3 ppb.yr^{-1}], the 1990s [4.9-6.5 ppb.yr^{-1}] and the 2000s [2.3-3.6 ppb.yr^{-1}] with mean values of 12±6 ppb.yr^{-1}, 6±8 ppb.yr^{-1}, 2±3 ppb.yr^{-1}, respectively. The associated uncertainty represents the 1-sigma variation from one year to another (inter-annual variability). The difference in the decadal growth rates between the four networks is less than 1 ppb.yr^{-1}.

ST2 - Regional and latitudinal distributions of wetland and biomass burning emissions (Figure S0 and S1)

Using the different top-down and bottom-up models and inventories gathered in this work, we computed averaged maps (Fig. S0) and zonally averaged emission fluxes of CH_4 from natural wetlands (Fig. S0 & S1, top), and biomass-burning (Fig. S0 & S1, bottom). To calculate the mean emissions we used the following time periods: 1990-2006 for wetland emissions and 1980-2006 for biomass burning emissions. As a result, the FINN inventory is not included in Fig S0 and S1. Averaged spatial pattern present common zones of emissions (stippled points on the right panels of Fig. S0): 66±9% for wetland emissions and 38±9% for biomass burning emissions. In Fig. S1, the bottom-up zonal means are presented as coloured solid lines whereas for top-down, only the range (min-max) is shown with the coloured areas. Wetland emissions are mainly located in the Tropics and in the high latitudes. ORCHIDEE's estimates are higher and with more spatial variations than those of LPJ except below 30°S. In the Tropics, LPJ's estimates by 1° band of latitude are around 10-20 Tg/yr, generally below ORCHIDEE's estimates. In the mid and high latitudes, the B-U models show a larger spread. In particular, the ORCHIDEE-P07 estimate is much higher than any other estimate (including ORCHIDEE-TOP) around 45°N and north of 60°N. LPJ-wsl follows ORCHIDEE-P07, but only up to 57°N. This shows that the wetland emission estimate is highly sensitive to the wetland extent, which remains a challenge for modellers. The top-down estimates are generally in the lower range of the bottom-up values, except around 30°S. Regarding the top-down range, the minimum is mainly due to the estimates from GEOS-Chem while the Carbon-Tracker-CH_4 model retrieves the highest estimates, except north of 60°N where LMDZt-SACS is the highest. The biomass burning emissions, including biofuel, occur essentially in the Tropics where the highest fluxes are found along with a great spread between the models. Note the different scale compared to the wetland emissions. For biomass burning emissions, the ranges of estimates from top-down are similar to the bottom-up estimates. The model LMDZ-MIOP produces the maximum observed in the Tropics. The lowest estimates come from the GEOS-Chem model. The other top-down models lie in-between. In the mid latitudes, CH_4 emissions from biomass burning and biofuel essentially originate from biofuel burning.

ST3 - Time series of CH_4 emissions from natural wetlands and biomass-burning for northern regions and tropical regions (Figures S2 and S3)

Deseasonalized time series (12 month running means) for CH_4 emissions from natural wetlands (top, in green) and biomass burning (bottom in red) are plotted in Fig. S2, for both the Tropics (<30°N, left) and the northern high latitudes (50-90° N, right). Lines represent the different bottom-up models. Coloured ranges represent the top-down inversions. Fig. S3 is the same as Fig. S2 for natural wetlands, but plots the anomaly computed as the deseasonalized time series minus the long-term mean of each time series. Fig. S2 illustrates the large uncertainties remaining in the estimation of the long-term mean emissions from natural wetlands and biomass burning in the Tropics. It also shows that a large climate event, such as the 1997-98 El Niño, can have a very different impact on biomass burning among models. Fig. S3 shows that the IAV of CH_4 emissions from natural wetlands is more robustly estimated than the long-term mean. There is a better agreement on the phasing of year-to-year changes among studies than on their magnitude. Most approaches show an increasing long-term trend for CH_4 emissions from natural wetlands since the mid 1990s.

ST4 - Latitudinal distribution of the IAV of emissions and sinks (Figure S4)

Figure S4 shows the latitudinal distribution of the inter-annual variability of emissions and sinks. For both the emissions and the sinks, we calculated the 12-month running means of monthly zonal mean for band of 1 degree of latitude. For the emissions, in order to avoid interpreting long-term changes and focus on year-to-year changes, we subtracted a linear trend from the deseasonalized zonal means. The inter-annual variability was then defined as the standard deviation of the de-trended time series of the deseasonalized zonal means over the period 1995-2005. This calculation was possible for all approaches except those providing only yearly data.

For the CH_4 loss, we applied a slightly different calculation in order to allow comparison to the IAV estimates performed in Montzka et al. (2011)[29]. Instead of expressing the anomaly as the standard deviation of the deseasonalized zonal mean, we defined the IAV as the difference between monthly deseasonalized zonal mean and long-term mean. This calculation enhances the estimated IAV by 0.1-0.4%.

Over the three decades, natural wetland variability dominates the year-to-year changes in emissions with a tropical maximum spread between 30°S and 30°N, and a secondary maximum at northern latitudes around 50°N (Fig. S4-a). The magnitude of the year-to-year variability of other emissions is 4-8 times smaller than for natural wetlands (Fig. S4-b-d), except for biomass burning due to the 1997-98 El Niño (Fig. S4-b). Fossil fuel IAV dominates at mid latitudes of the northern hemisphere (fig. S4 c) and produces a secondary peak in the zonal average of CH_4 emission IAV at 30°S. Both regions are home to most of the developed countries (northern hemisphere, mid-latitudes) and some rapidly developing tropical countries in Southeast Asia, South America, Central Africa, and Oceania. The bottom-up inventories produce a third intriguing peak of fossil CH_4 emission IAV in the high northern latitudes, not consistent with the observation-driven top-down inversions. IAV of agriculture/waste emissions (Fig. S4-d) from top-down is largest between 10°N and 40°N where most of the rice agriculture and waste production from animal husbandry in China, India and South-East Asia are located. OH IAV is largest in the Tropics (Fig. S4-e,f) where most of the OH is produced. Top-down inversions are more in agreement in the 2000s than in the 1990s with bottom-up models as explained in the main text.

ST5 - Year-to-year variations of emissions (Figure S5)

Figure S5 represents the evolution of the anomalies of each emission category over the last three decades. The emission anomalies were calculated as the difference between deseasonalized emissions (12-month running mean), and the long-term mean of the emissions. A consistent period for estimating the long-term mean is not suitable to all the data sources. As a result, the long-term mean was calculated as the mean emission over the stable period 1999-2006, except for wetland (1985-2006) and for fossil fuel and agriculture/waste inventory estimates (1990-2006). For studies covering shorter time periods (mainly in the 2000s), the long-term mean was calculated over the period 2000-2006. For studies starting after the year 2000, the time period used for calculating the long-term mean was reduced accordingly (e.g. TM5-4DVAR: 2003-2009). The ranges of the anomalies given in the main text are consistent with those presented in Figure S5.

The IAV of CH_4 emissions and sinks is defined by year-to-year fluctuations, superimposed on decadal trends (see main text for the decadal trend analysis). Over the three decades, natural wetlands dominate the year-to-year emission variability (Fig. S4). Bottom-up and top-down generally agree on this result, although different models compute different IAV magnitudes (Fig. S5). Bottom-up models for wetland emissions, for instance, may differ in their estimation of year-to-year changes, mainly because of different: 1) spatial distribution of emissions (Fig. S0), 2) structure and parameter values of wetland extent and CH_4 production, oxidation and transport processes, and 3) modelled sensitivity of enzyme kinetic and microbial processes to temperature and precipitation. For instance, the IAV of wetland extent is not fully represented in all wetland-emission models.

Two large events are driving the observed year-to-year changes in the atmosphere during the 1990s (Fig. S5): The Mount Pinatubo volcanic eruption in the Philippines (June 1991) and the large El Niño

Southern Oscillation event of 1997-98. The Pinatubo volcanic eruption induced a large seesaw in the CH_4 growth rate. The initial increase in the growth rate in 1991 was likely caused by the negative impact of volcanic SO_2 and aerosols on OH production, which may have decreased by 3-5%[10,30]. The subsequent cooling of the northern hemisphere (NH) following the eruption reduced CH_4 emissions from wetlands from 1991-93 by 13[3-21] Tg of CH_4 for top-down and 15[9-23] Tg of CH_4 for bottom-up models, with 67-75% of the emission perturbation located in the Tropics. This consequently decreased the atmospheric growth rate in 1992-93. The economic collapse of the former USSR also impacted the growth rate in 1991 and during the following years[31,32,66] with stagnant anthropogenic emissions at global scale estimated by both top-down and bottom-up.

The large El Niño Southern Oscillation event of 1997-98 also affected the CH_4 IAV. At that time, widespread dry spells caused increased fire activity in the tropics and in boreal regions of Eurasia[33,34] and reductions in natural wetland emissions. Above-average biomass-burning emissions of up to 21[8-32] Tg of CH_4 for bottom-up and 10[5-25] Tg of CH_4 for top-down are estimated for 1997-1998, mostly (85-90%) in tropical regions (Fig. S1 and S2). The 1997-98 large positive anomaly in biomass-burning emissions is on average two times more prominent in the bottom-up approach than in top-down inversions, possibly due to the lack of atmospheric measurements near the Indonesian peat fires attributing the CH_4 anomaly to other regions or sources, or due to dilution by fast vertical mixing. Natural wetland emissions from bottom-up and top-down consistently show a northern hemisphere-driven reduction in 1997 of 9[4-12] and 6[1-19] Tg of CH_4 respectively, followed by a tropical-driven increase in 1998 of 16[9-23] and 17[12-20] Tg of CH_4, respectively (Fig. S5 and S2).

ST6 – IAV variations of sinks

As with the Pinatubo eruption, climate variability can impact the IAV of the chemical destruction of CH_4 by OH radicals. Fluctuations in OH concentration could explain a large part of the observed variability of atmospheric CH_4. Typically, a 1% change in global OH concentration impacts the global CH_4 budget by up to 5 Tg of CH_4. The analysis of top-down inversions and bottom-up CCM results reveals a much better agreement for the IAV of CH_4 loss by OH in the 2000s compared to the 1990s

(Fig. S4-e, f): a maximum of IAV is found in the tropics (Fig. S4), and the global IAV of CH_4 loss by OH is 0.9 and 0.4% for two of the top-down inversions, and 0.9, 0.5 and 0.4% for the three CCMs providing a full IAV analysis. Indeed, the mean IAV of the CH_4 chemical loss computed from ACCMIP models is 0.4±0.2%. This value is to be considered as a lower limit because time-slices only account for internal variability of the models as emissions and sea surface temperatures are constant within each time-slice. GISS and LMDzORINCA provided transient runs so the calculated inter-annual variability is somewhat more complete, although annual emissions are interpolated between varying emissions between decades. The TM5 model provided results with full representation of IAV. For these three models, IAV is estimated at 0.5% and 0.4% and 0.9% respectively as mentioned above. These values are the largest of the CCM models used in this work. Without these two models, the IAV decreases to 0.3±0.2%, suggesting that at least half of the IAV of the CH_4 chemical loss is due to IAV in trace gas and aerosol emissions.

This small IAV during the 2000s, with top-down inversion IAV still twice that of the CCMs, is consistent with recent estimates of OH concentration IAV since 1998 reported to be less than 5% when using a box model and less than 3% when using a three dimensional top-down inversion with an estimate of 1.8±1.2%[29]. The large IAV of CH_4 loss by OH before 1998 is now analysed as an artefact of the overly large sensitivity of OH concentration inferred from methyl chloroform measurements to uncertainties in its emissions[29]. An alternative scenario invokes the occurrence of several large El Nino events[35] before 1998. Finally since 2007, as for the CH_4 sink, year-to-year changes in OH concentrations are found to be small[29,36](< 1% per year), and possibly partially offset by the increase of atmospheric CH_4[37].

In addition, even if ACCMIP models simulate IAV, we cannot discuss specific climate events using the ACCMIP CH_4 chemical loss because the climate models used for the simulations are not nudged to meteorological reanalyses. Meteorology depends on the climate that is being simulated in the climate portion of the models, which will show year-to-year variations, but not necessarily in phase with observed climate events such as El Niño. Finally, only two top-down inversions provided OH fields to calculate IAV, which explains why only two estimates are shown.

ST7 - A simple model for CH_4 emissions from termites (Figure S6)

Several up-scaling approaches have been carried out to quantify the global contribution of termites to CH_4 emissions[38-40]. However, although the number of available information is increasing, estimates still show large uncertainties, related to: 1) the effect of soil and mound environments on net CH_4 emissions, 2) the quantification of termite biomass for each ecosystem type, and 3) the impact of land use change on termite biomass.

We have computed CH_4 emission from termites at global scale as the product of termite biomass (derived by gross primary production, as proxy of net primary production for tropical ecosystems), a termite emission factor (fix), and a crop reduction effect (fix). Using as input global GPP products (GPP_{MET}[41,42]) and crop distribution maps[43] (new version of Ramankutty and Foley, 1999; http://www.geog.mcgill.ca/~nramankutty/Datasets/Datasets.html) from 1982 to 2007, the equation in Fig. S6 was applied in a GIS environment to obtain yearly CH_4 emission estimates. First, the GPP of the "Other-Than-Crop" (OTC) land covers was extracted from $GPP_{MET,}$ and termite biomass (g m^{-2}) was calculated. Termite biomass in the crop area was estimated to be 40% of the original pristine ecosystem, whereas no consistent effect from conversion into pastries and secondary forests was found [44-47]. Total biomass (Tg of CH_4 per year) per pixel was then aggregated on the basis of natural vegetation classification[43] for land regions between 35°S and 35°N. To calculate CH_4 emissions outside ± 35°, i.e. temperate forests, temperate grasslands, and Mediterranean shrublands, the total suitable land surface (10^6 km^2) was multiplied with a termite biomass value of 3.0 g m^{-2} for temperate ecosystems[38], and 4.0 g m^{-2} for Mediterranean areas (average value derived from GPP of Australian mallee areas and data reported for a similar Australian ecosystem[48]).

Based on a literature analysis[38,49-51], we used a CH_4 emission factor of 2.8 ± 1.0 mg CH_4 (g^{-1} termite) for tropical and Mediterranean ecosystems. For temperate forests and grasslands we use the value of

1.7 mg CH_4 g^{-1} termite[52]. No significant conversion of natural ecosystems into crops was assumed in these areas during the period 1980-2009.

Yearly CH_4 emissions (g m^{-2} y^{-1}) were finally computed and averaged over three periods 1982-1989, 1990-1999 and 2000-2007 representative of the 1980s', 1990s' and 2000s', respectively. We find 8.7±3.1 Tg of CH_4 per year for the 1980s, 8.7±3.1 Tg of CH_4 per year for the 1990s, and 8.8±3.2 Tg of CH_4 per year for the 2000s. The uncertainty of the total estimate was calculated 1) by applying error propagation of products to calculations, which included main variables (termite biomass, CH_4 emission factor, and land use effect), and 2) by means of error propagation of the sum when global estimates of CH_4 were computed. These estimates are in the lower bound of current estimates and show only little inter-annual variability. Regionally, tropical South America and Africa are the main sources (36 and 30% of the global total emission, respectively) due to the extent of their natural forests and savanna ecosystems.

ST8 - The "plant" source

After the 4th IPCC Assessment Report one study concluded that plants were able to emit CH_4 under aerobic conditions contributing a moderate-to-large global source of 62-236 Tg of CH_4 per year to the global CH_4 budget[53]. This finding was consistent with the first maps of column CH_4 retrieved from the SCIAMACHY space-borne instrument that revealed a large excess of CH_4 above tropical forests[54], although not in agreement on the magnitude of potential plant emissions. However, this correlation appeared to be fortuitous. Indeed, later improvements to the spectroscopy led to large reductions of the satellite-observed atmospheric CH_4 excess in the tropics[55]. Although plants may emit CH_4 under aerobic conditions, additional measurements on plant emissions[56-59] and atmospheric analyses[60] have not supported that plants, under aerobic conditions, are a significant player in the global CH_4 budget.

I.2 Supporting figures

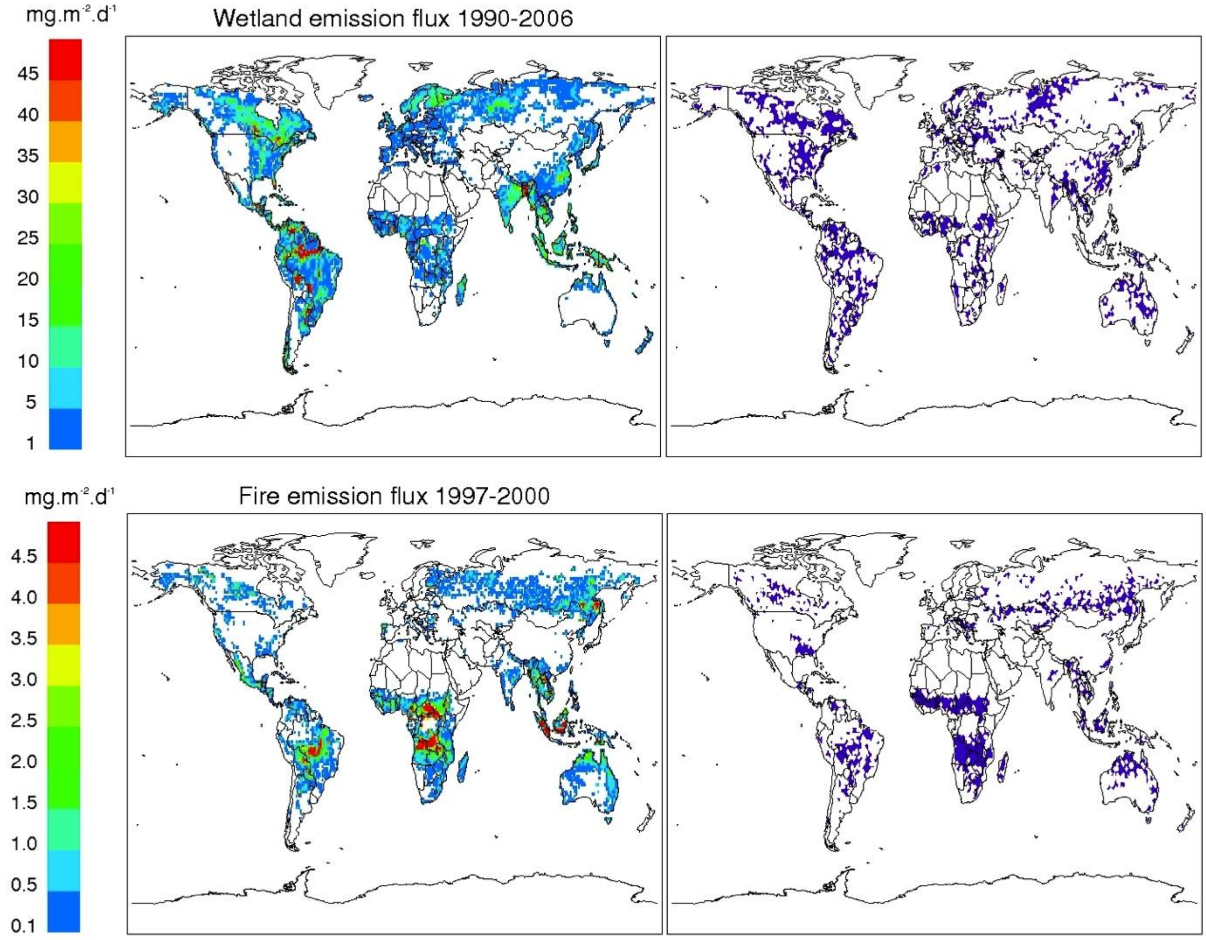

Figure S0: (Left) Distribution of methane emissions from natural wetlands (top) and fires (bottom) at 1x1° resolution in mgCH_4/m^2/day. Note the different color scales. Emissions lower than 1 mgCH_4/m^2/day (0.1 for fires) are not shown. Each map is an average over the maximum common period of time of the different models aggregated in this study. On the right, purple areas indicate grid cells where the mean emission is larger than the standard deviation between the B-U studies aggregated to build the map.

s

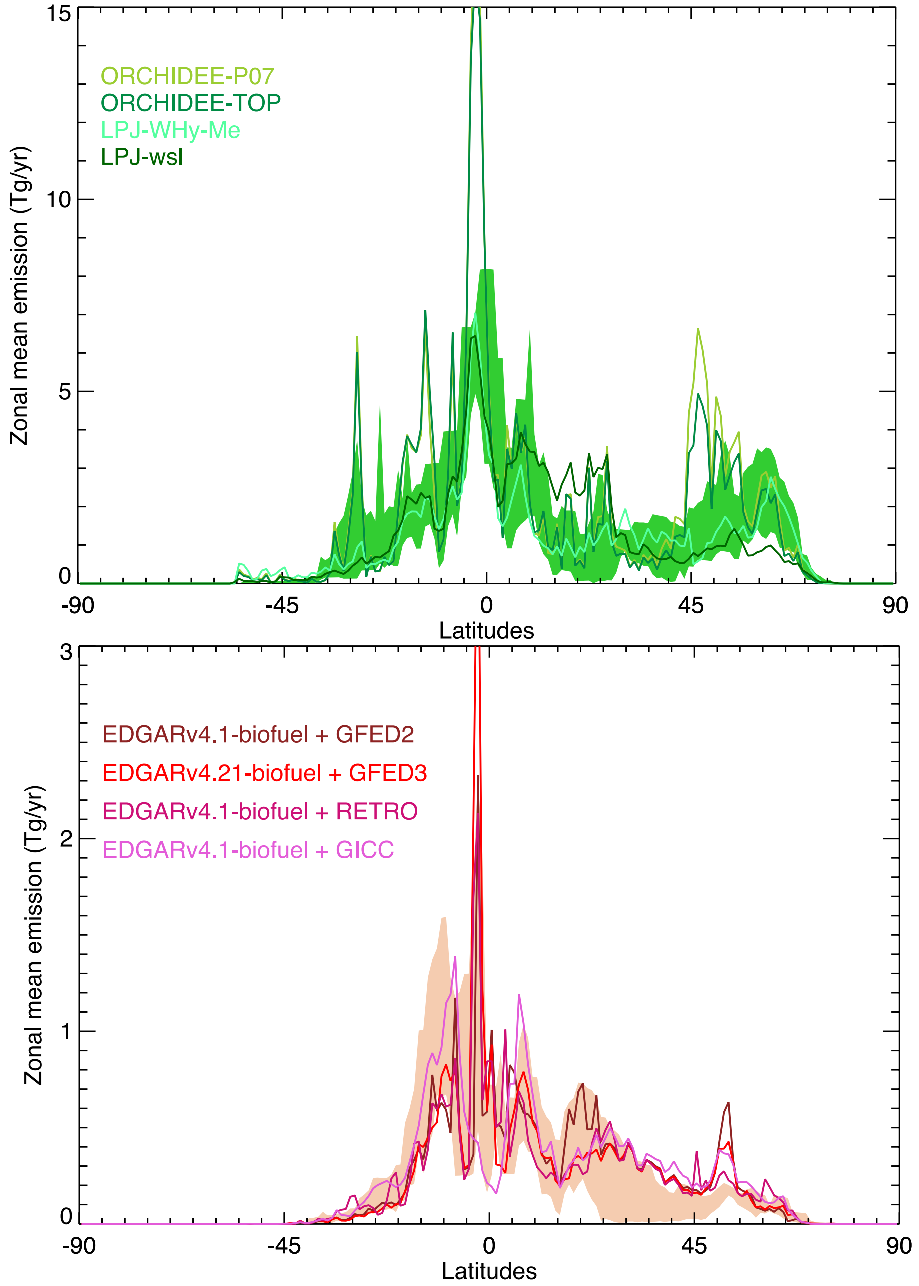

Figure S1: Zonal mean fluxes of CH_4 from natural wetlands (top), biomass burning (including biofuel, middle), and OH loss (bottom). The zonal mean has been computed over the period 1990-2006 for wetland emissions and 1980-2005 for biomass burning emissions. The coloured lines correspond to B-U models or inventories as specified in the legend (the same as those used to compute the gridded maps in Fig. S0). Coloured ranges indicate the minimum and maximum of the zonal mean fluxes derived from T-D inversions. Zonal mean of methane loss through OH oxidation is computed by the ACCMIP models and the T-D inversions (PYVAR and LMDZ-MIOP), temporal average being calculated over the 2000s. Note that vertical scales are different for the three plots.

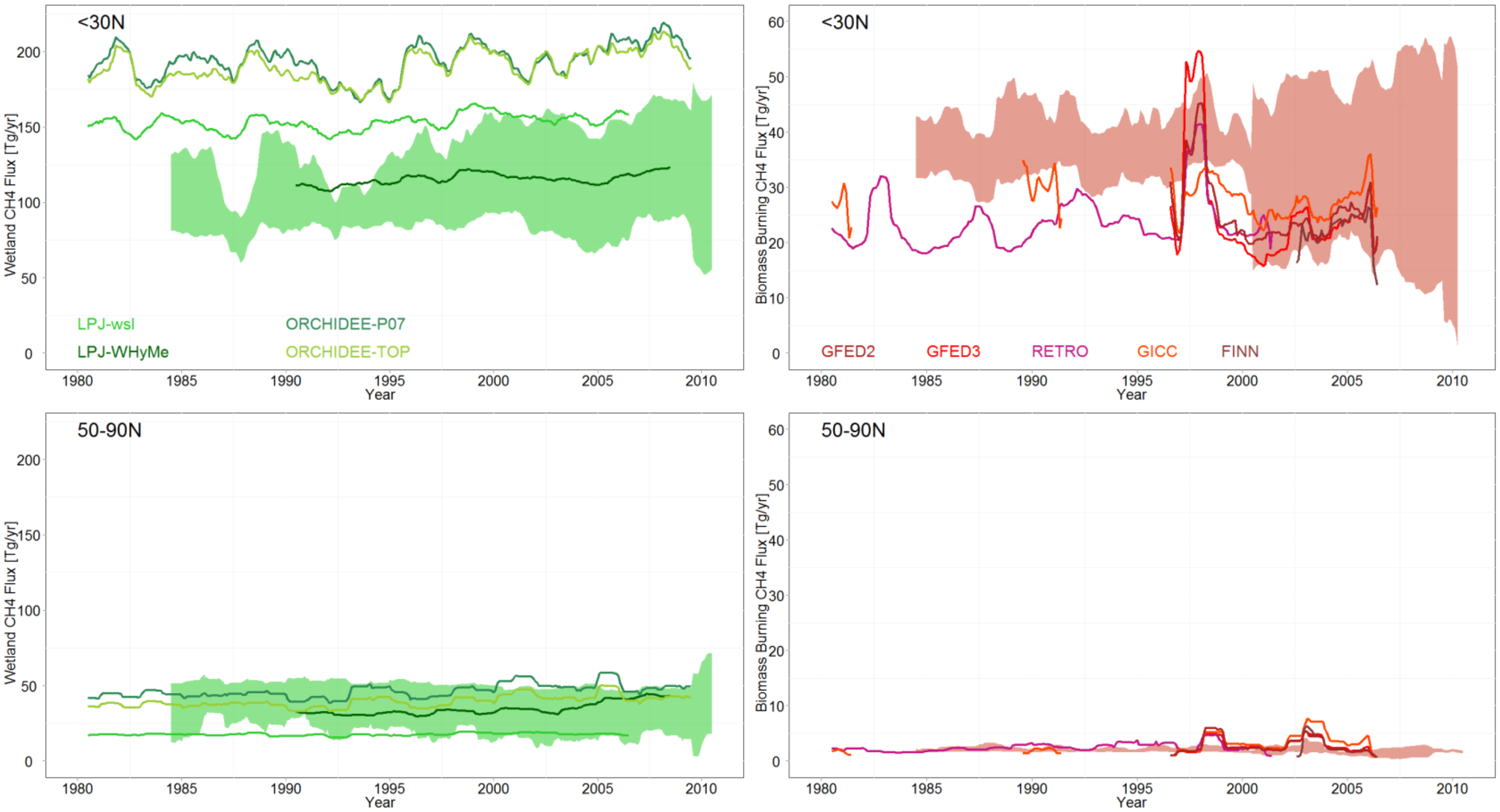

Figure S2: Deseasonalized CH_4 emissions from natural wetland emissions (top, in green) and fires (bottom, in red) for two latitudinal bands (Left: Tropics <30°N, Right: Northern latitudes, 50-90°N). Lines represent B-U models and inventories. Colored ranges are for T-D inversions. Wetland emissions are from ORCHIDEE[61], LPJ-WHyMe[62] and LPJ-WSL[63], and inversions[36,64-66]; biomass-burning emissions are from RETRO[67], GFEDv2 [68], GFEDv3[34], GICC[69] and FINN [70], and inversions (same as for wetlands). Note that y-axis scales are different for wetland and biomass-burning emissions.

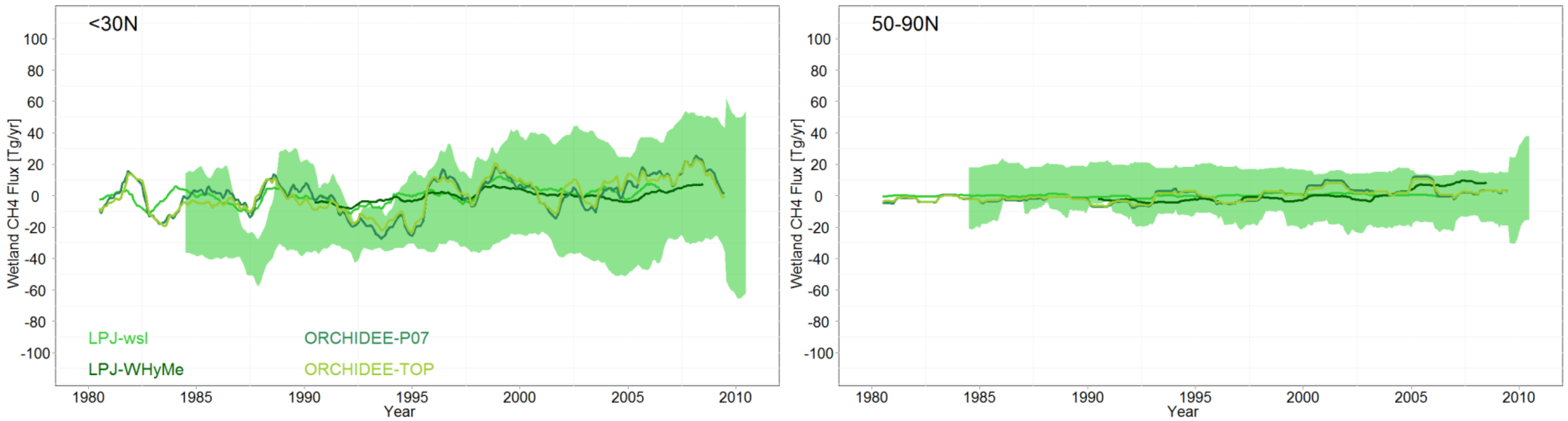

Figure S3: Same as figure S2 but for the anomaly (de-seasonalized time series minus their long-term mean) of CH_4 emissions from natural wetlands (in $TgCH_4.yr^{-1}$) for two latitudinal bands (Left: Tropics <30°N, Right: Northern latitudes, 50-90°N). Lines represent B-U models and inventories. Colored ranges are for T-D inversions.

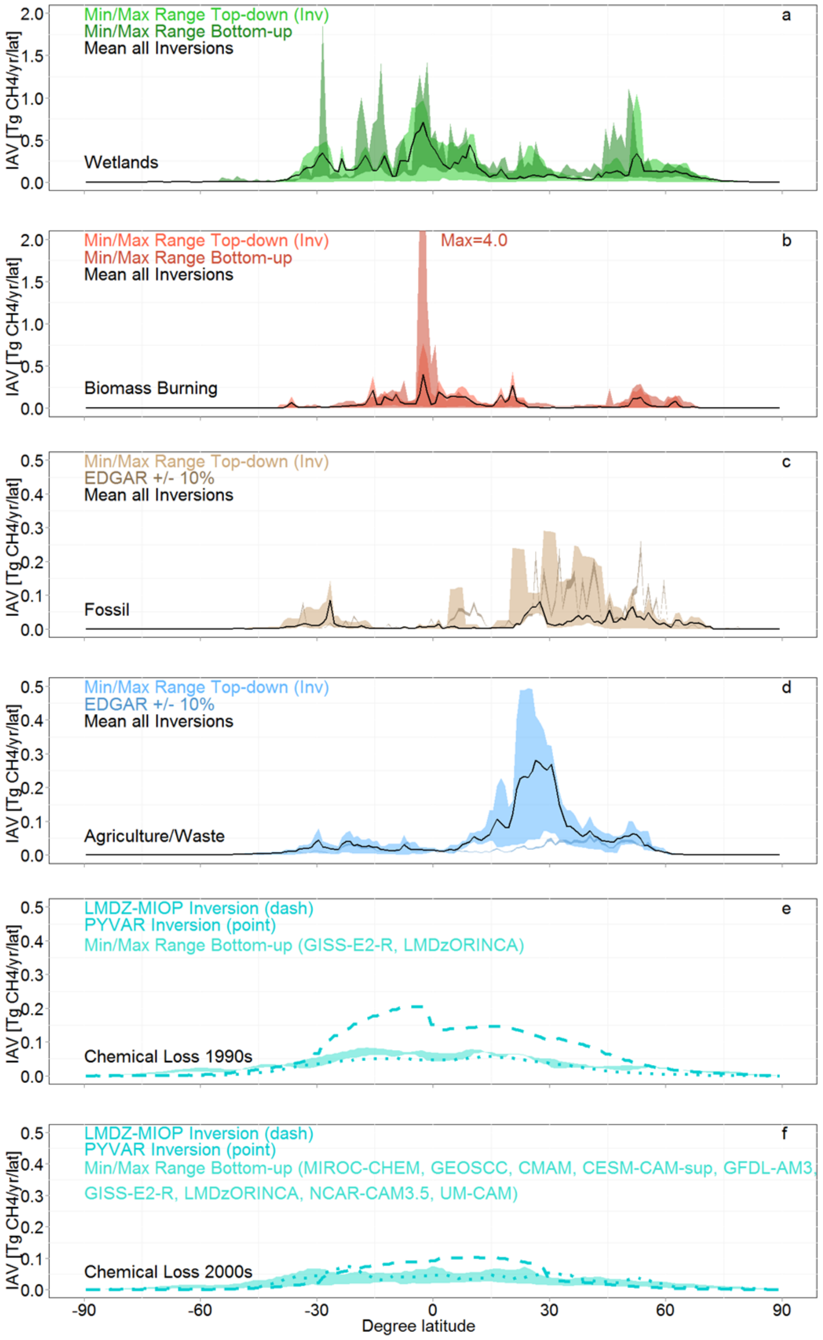

Figure S4: Inter-annual variability (IAV) of T-D and B-U emissions and sinks as a function of latitude. IAV is calculated as the de-trended standard deviation of the zonal emissions and sinks at 1° resolution. Range of all T-D inversions is shown as light coloured shaded area (except for chemical loss). Range of all B-U approaches is shown as dark-coloured shaded area (wetland models, fire models and inventories). From top to bottom: natural wetlands (green), fires (red), fossil fuels (brown), agriculture/waste (blue), and chemical loss (turquoise) for the 1990s and the 2000s. For chemical loss, T-D inversions are shown as lines. Note that y-axis scales are extended for wetland and biomass-burning emission IAV.

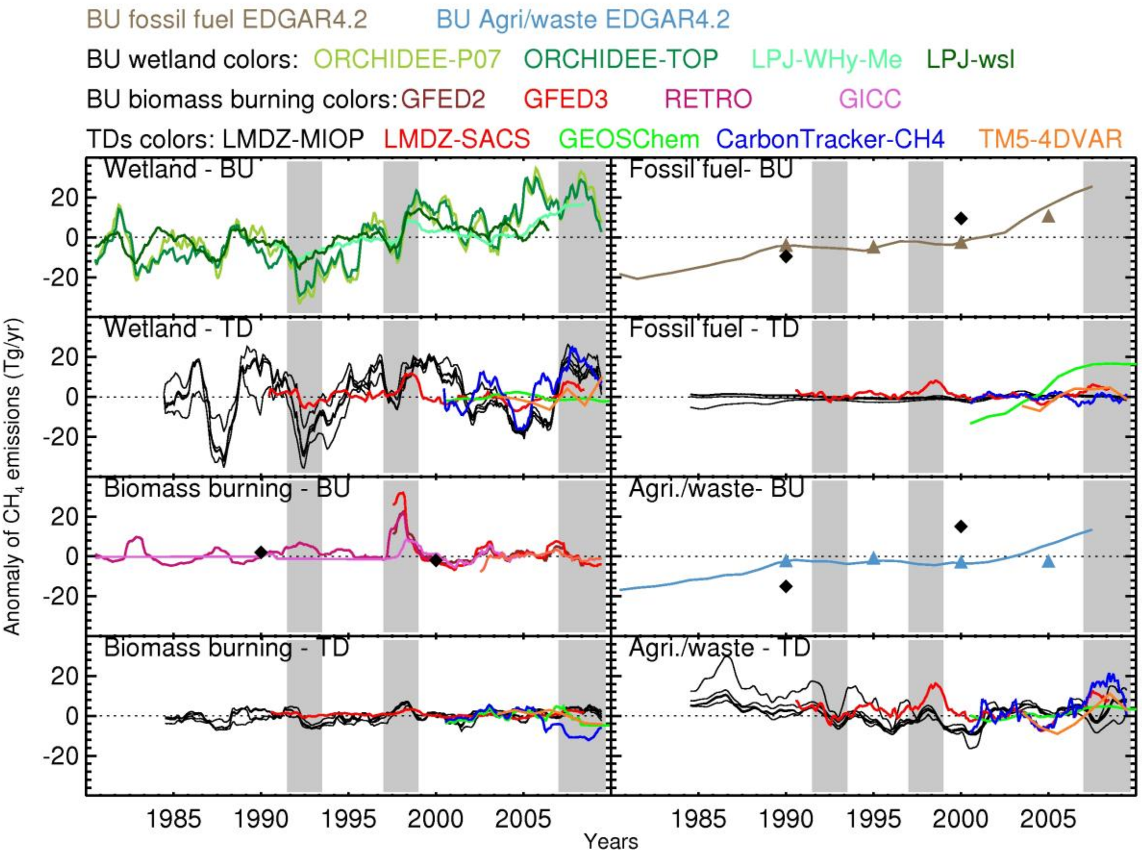

Figure S5: Inter-annual variability (IAV) of T-D and B-U emissions over the last three decades. Anomalies are calculated as the difference between deseasonalized emissions (12-month running mean), and a long-term mean of the same emission. Long-term mean is calculated as the mean emission over the stable period 1999-2006, except for wetland (both T-D and B-U, 1985-2006) and for fossil fuel and agriculture/waste inventories (1990-2006). For studies covering shorter periods the long term mean is based on a subset of the 1999-2006 period (except for TM5-4DVARbn 2003-2009). The decadal IIASA and EPA inventory values are represented as black diamonds and coloured triangles, respectively. The shaded grey areas highlight the three time periods discussed in the text (post-Pinatubo period, 1997-98 El-Nino, and the recent years).

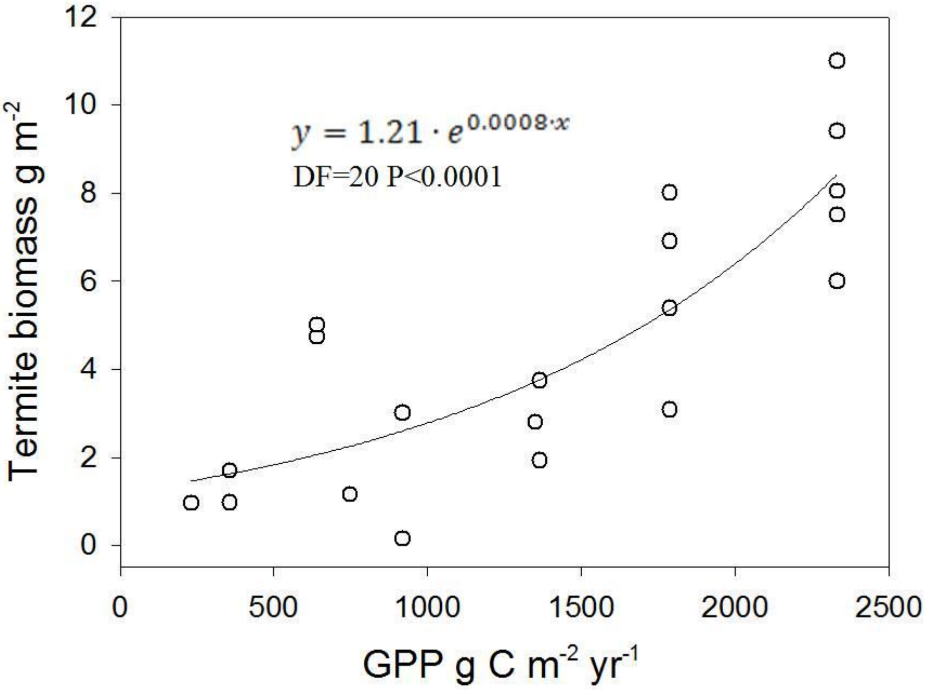

Figure S6: Termite biomass vs. mean annual GPP derived from different sources [71,72]*for tropical areas. Termites biomass data are extracted from the main published studies*[48,49,73-82].

I.3 Supporting tables

Table S1: T-D Model main characteristics

	TM5-4DVAR (Bergamaschi et al., 2009)	**LMDZ-MIOP (Bousquet et al., 2011)**	**CarbonTracker-CH4 (Bruhwiler et al., 2011)**	**GEOS-Chem (Fraser et al., 2011)**	**TM5-4DVAR (Houweling et al., 2012)**	**LMDZt-SACS (Pison et al., 2009, Bousquet et al., 2011)**	**GCM used by Fung et al., 1991**	**TM2 (Hein et al., 1997)**	**MATCH (Chen & Prinn, 2006)**
Data sets (indicate network/instrument)									
Satellite	IMAPv5.5 retrievals (Frankenberg et al., 2011)[1]	/		/	SCIAMACHY IMAPv5.5	/		/	/
Ground based	NOAA / ESRL (only marine and continental background sites)	MCF=AGAGE CH4=CSIRO, NOAA, LSCE	NOAA-ESRL and Environment Canada sites (88 sites)	48 ESRL sites	NOAA-ESRL	MCF=NOAA, AGAGE, CH4=CSIRO, EC, NOAA, RAMCES, NIWA, AGAGE (continuous), SAWS, INMA, ENEA, JMA, UBAG	NOAA/CMDL (19 sites), CSIRO (2 sites), 2 additional sites (Cape Point, South Africa; Tsukuba, Japan)	NOAA (30 stations for CH4) 13CH4 observations (6 stations from UCI, and 1 from NIWA)	NOAA (54 flask sites) AGAGE (5 high frequency sites)
Satellite + Ground based	bias correction of satellite data (2nd order polynomial as function of latitude and month) (Bergamaschi et al., JGR, 2009)	/		/	SCIAMACHY inversions are always carried out in combination with surface data	/		/	/

Prior scenarios									
Emissions	anthropogenic emissions (except biomass burning): EDGARv4.1, biomass burning: GFEDv3.1, wetlands: inventory from Jed Kaplan (Bergamaschi et al., JGR, 2007), further minor natural sources as described in (Bergamaschi et al., 2009)	MCF=Montzka et al., 2000 + Bousquet et al., 2006, CH4= EDGAR 3.2, GFED-v2 (van der Werf et al., 2006), Matthews et Fung (1987)	EDGARV3.2, GFED3, Bergamaschi et al. 2007 wetlands	ruminant animals, coal mining, oil production, landfills: EDGAR 3.2 FT (Olivier et al., 2005); biomass burning: GFEDv2 (van der Werf et al., 2006); oceans: Houweling et al., 1999; wetlands and rice: Bloom et al., 2010; termites, hydrates: Fung et al., 1991	EDGARv4.1 (Anthropogenic), GFED3 (BMB), LPJ-WhyMe (Wetlands) + minor processes	MCF=Montzka et al., 2000 + Bousquet et al., 2006, CH4= EDGAR 3, GFED-v2 (van der Werf et al., 2006), Fung et al. (1991), constant over the oceans	Wetlands: Matthews and Fung, 1987; rice: Matthews et al., 1991; animals: based on Crutzen et al., 1986 and Lerner et al., 1988; natural gas: U.S. Department of Energy, 1986, U.N. Department of International Economic and Social Affairs, 1986; coal: Espenshade, 1978, Central Intelligence Agency, 1978 and 1986, Seydliyz Weltatlas 1984, U.N. Department of International Economic and Social Affairs, 1986; biomass burning: Houghton et al., 1987; termites: based on Matthews, 1983, Zimmermann et al., 1982 and 1983, Fraser et al., 1986; hydrates: based on Kvenvolden, 1988	Based on Fung et al., 991	Adapted from Fung et al., 1991 For wetland and rice EDGAR3.0 for anthropognic Hao and Liu [1994] for biomass burning

Sinks	troposphere: TM5-OH (Bergamaschi et al., 2009), stratosphere: OH, O(1D) and Cl from 2D MPI model (Brühl and Crutzen, 1993), soil sink: (Ridgwell et al., 1999)	Prior OH Field from MOZART model (Hauglustaine 2004)	troposphere: TM5-OH (Bergamaschi et al., 2007), stratosphere: OH, O(1D) and Cl from 2D MPI model (Brühl and Crutzen, 1993), soil sink: (Ridgwell et al., 1999)	OH: 3D monthly fields from a full-chemistry Ox-NOx-VOC run of the GEOS-Chem model (Fiore et al., 2003); soil sink: Fung et al. 1991; stratospheric loss: adapted from a 2-D stratospheric model (Wang et al., 2004)	Climatological OH based on Montzka, Science, 2011	Prior OH fields by INCA	OH: Spivakovsky et al., 1990a,b; soils: based on Born et al., 1990 and Matthews, 1983	OH Computed with the chemistry-transport model of the paper	OH output of a T62 run of the MATCH model,
Meteorological forcing	ECMWF Era-Interim	LMDZ on-line nudged on ERA40	ECMWF Forecast	GEOS5	ECMWF ERA-interim	LMDZ on-line nudged on ERA40	Hansen et al., 1983	ECMWF analysis	NCEP reanalysis
Model characteristics									
Resolution (lonxlatxlev)	6x4 degrees; 25 vertical layers	3.75degreesx2.5degreesx19 sigma-pressure levels	6x4 degrees, 25-34 levels	5x4x47	6x4x25 (degree lon, degree lat, # layers)	3.75degreesx2.5degreesx19 sigma-pressure levels	4x5 (degree lat, degree lon), 9 vertical layers	7.5x7.5 (degree lat, degree lon), 14 vertical layers	1.8x1.8 lat, degree lon), 28 vertical layers
PBL scheme	Holtslag and Moeng, 1991]	Local closure	Holtslag and Moeng, 1991	VDIFF (Lin & McElroy, 2010)	Holtslag & Moeng (J. Atmos. Sci., 1991)	Local closure		Local closure based on Louis, 1979	
Convection scheme	Tiedke, 1989	Tiedtke et al., 1989	Tiedke, 1989	Relaxed Arakawa-Schubert scheme (Moorthi and Suarez, 1992)	Tiedtke (Mon. Wea. Rev., 1989)	Tiedtke et al., 1989	Arakawa scheme B	Tiedtke et al., 1989	
Inversion									
Time resolution (flux domain)	monthly	one month	Weekly aggregated to monthly	8 day	monthly	one week		monthly	Monthly

Spatial resolution	grid cell (6x4 degrees)	10 land regions + 1 ocean region	120 land regions based on source process and Transcom region, 1 ocean	Based on Transcom (Gurney et al., 2002): 99 land regions + 11 ocean regions + 1 ice region	6x4 degree	grid cell (3.75 °x2.5°)		Global per process	Large regions and processes
Correlation length (flux domain)	500 km	/		/	1000 km	500 km on land, 1000 km on ocean		/	
Minimizer	m1qn3	Analytical solution	Ensemble Kalman smoother	ensemble Kalman filter	Variational approach	m1qn3	/	/	Kalman filter
Time window	2003-2010	1983-2010	2000-2011	2000-2010	2003-2010	1990-2008	1980-1989	1983-1989	1996-2001

Table S2: Estimated CH_4 fluxes corresponding to the regional bar plots in Fig. 3. Values are given in Tg yr^{-1} (**mean** [min-max]) for the 2000s.

Region		Wetlands	Biomass-burning	Fossil Fuels	Agriculture/ Waste	Other Sources	Soil Sink	OH Chemical Sink
Africa	T-D	**36** [20-48]	**9** [7-14]	**7** [3-13]	**18** [16-22]	**9** [7-15]	**8** [5-12]	**43** [NA]
	B-U	**24** [22-27]	**8** [6-12]	**9** [7-11]	**21** [13-29]	NA	NA	NA
Australia	T-D	**4** [0-11]	**0** [0-1]	**1** [0-2]	**3** [2-5]	**1** [1-2]	**2** [1-3]	**12** [NA]
	B-U	**3** [2-3]	**1** [0-2]	**1** [1-2]	**5** [4-6]	NA	NA	NA
China	T-D	**6** [2-12]	**1** [0-3]	**15** [9-21]	**29** [21-36]	**1** [1-2]	**2** [1-2]	**8** [NA]
	B-U	**7** [5-10]	**4** [4-5]	**12** [10-13]	**28** [25-31]	NA	NA	NA
Eurasia, boreal	T-D	**14** [9-23]	**1** [1-2]	**7** [3-11]	**2** [1-3]	**1** [0-1]	**3** [1-5]	**4** [NA]
	B-U	**9** [4-13]	**1** [1-2]	**11** [6-17]	**4** [2-6]	NA	NA	NA
Eurasia, temperate	T-D	**4** [0-13]	**0** [0-1]	**14** [9-17]	**13** [12-15]	**2** [1-3]	**2** [2-3]	**14** [NA]
	B-U	**2** [2-2]	**1** [0-1]	**15** [13-18]	**15** [15-16]	NA	NA	NA
Europe	T-D	**10** [4-19]	**0** [0-1]	**18** [7-23]	**20** [13-26]	**1** [1-2]	**2** [2-3]	**8** [NA]
	B-U	**10** [5-17]	**2** [0-2]	**17** [9-26]	**25** [22-28]	NA	NA	NA
India	T-D	**2** [0-4]	**1** [0-3]	**2** [2-4]	**27** [19-43]	**1** [1-1]	**1** [0-1]	**5** [NA]
	B-U	**9** [5-16]	**2** [2-2]	**2** [2-3]	**22** [20-24]	NA	NA	NA
North America, boreal	T-D	**9** [6-17]	**0** [0-1]	**0** [0-1]	**0** [0-1]	**1** [0-2]	**2** [1-2]	**3** [NA]
	B-U	**16** [9-28]	**0** [0-1]	**1** [0-2]	**1** [0-2]	NA	NA	NA
North America, temperate	T-D	**8** [6-11]	**0** [0-1]	**18** [8-27]	**24** [21-31]	**2** [1-3]	**3** [2-4]	**13** [NA]
	B-U	**17** [10-29]	**1** [0-1]	**14** [13-15]	**21** [21-21]	NA	NA	NA
South America, temperate	T-D	**19** [10-32]	**2** [0-3]	**1** [0-2]	**19** [16-23]	**2** [2-3]	**3** [1-4]	**15** [NA]
	B-U	**23** [17-31]	**1** [1-2]	**1** [1-2]	**11** [6-17]	NA	NA	NA
South America, tropical	T-D	**28** [17-48]	**5** [3-9]	**2** [1-3]	**7** [6-9]	**4** [3-7]	**2** [0-4]	**16** [NA]
	B-U	**58** [39-92]	**4** [2-4]	**3** [3-3]	**15** [7-23]	NA	NA	NA
South East Asia	T-D	**19** [7-32]	**4** [3-6]	**4** [2-6]	**18** [10-32]	**2** [1-4]	**1** [0-2]	**10** [NA]
	B-U	**26** [14-37]	**5** [2-7]	**4** [3-5]	**21** [19-24]	NA	NA	NA

Table S3: Estimated regional CH_4 fluxes for each model corresponding to bar plots in Fig. 3. Values are given in Tg yr^{-1} for the 2000s.

	LMDZ-MIOP (Bousquet et al., 2011)	**TM5-4DVAR (Houweling et al., 2012)**	**CarbonTracker-CH_4 (Bruhwiler et al., 2011)**	**TM5-4DVAR (Bergamaschi et al., 2009)**	**GEOS-Chem (Fraser et al., 2011)**	**LMDZt-SACS (Pison et al., 2009; Bousquet et al., 2011)**	**LPJ-wsl (Hodson et al., 2011)**	**LPJ-WhyMe (Spahni et al., 2011)**	**ORCHIDEE (Ringeval et al., 2011)**	**GFEDv3 (Van der Werf et al., 2010)**	**RETRO (Schultz et al., 2007)**	**GICC (Mieville et al., 2010)**	**FINNv1 (Wiedinmeyer et al., 2011)**	**GFEDv2 (Van der Werf et al., 2004)**	**EDGARv4.1 (EDGAR4.1, 2009)**	**EPA, 2011**
North America, boreal																
Wetland	9.0	5.9	6.6	8.1	5.7	17.0	10.8	9.2	28.3							
Biomass Burning	0.5	0.7	0.3	0.6	0.3	0.3				0.5	0.6	0.7	0.2	0.3		
Fossil	1.0	0.4	0.2	0.2	0.3	0.9									0.1	2.2
Agriwaste	0.8	0.6	0.2	0.4	0.3	0.4									0.2	2.3
Other	0.3	1.6	0.4	0.9	0.6	0.2										
Soil	-1.8	/	-0.8	-1.1	-2.3	/										
North America, temperate																
Wetland	7.6	7.1	8.9	7.2	10.8	7.4	9.8	11.2	28.8							
Biomass Burning	0.9	0.2	0.2	0.5	0.2	1.0				0.6	1.2	1.5	0.9	0.8		
Fossil	27.2	15.9	8.0	14.1	15.0	25.8									13.4	14.8
Agriwaste	20.8	23.4	31.3	21.8	23.8	25.5									20.7	20.9
Other	1.1	3.2	0.8	1.3	1.4	1.2										
Soil	-2.8	/	-2.8	-3.9	-2.5	/										

South America, tropical

Wetland	20.4	26.6	28.8	47.5	29.8	16.8	38.6	42.4	92.1							
Biomass Burning	9.4	4.2	3.1	3.1	2.9	8.4				2.5	3.4	3.8	4.5	4.1		
Fossil	1.1	2.4	0.7	2.8	1.2	1.8									2.8	3.0
Agriwaste	6.8	6.1	8.6	7.9	6.3	7.6									7.1	22.8
Other	3.2	6.8	4.9	4.9	2.9	2.6										
Soil	-0.9	/	-3.0	-3.6	-0.4	/										

South America, temperate

Wetland	20.3	10.2	31.9	16.7	15.0	21.4	16.7	20.9	31.1							
Biomass Burning	3.0	1.7	0.5	1.5	1.2	3.0				1.0	2.0	2.4	1.0	1.0		
Fossil	1.0	2.0	0.5	1.9	1.2	0.9									2.1	0.7
Agriwaste	16.8	20.8	22.6	20.3	15.9	18.3									17.2	5.6
Other	2.0	3.3	2.2	2.8	2.1	2.1										
Soil	-1.6	/	-3.6	-4.3	-0.9	/										

Europe

Wetland	10.4	5.0	6.8	3.8	15.4	18.8	4.8	16.7	9.4							
Biomass Burning	1.1	0.2	0.2	1.0	0.2	0.7				1.8	1.9	0.4	2.1	1.8		
Fossil	23.0	21.1	19.0	18.3	7.4	20.3									25.9	8.8
Agriwaste	22.3	14.9	26.0	13.3	18.6	22.8									27.6	22.0
Other	0.8	2.0	0.9	0.8	1.2	0.6										
Soil	-2.2	/	-2.3	-1.7	-2.9	/										

Africa

Wetland	36.2	20.4	46.2	44.7	47.8	19.7	22.1	23.7	27.4							

Biomass Burning	13.9	7.6	6.7	8.3	7.3	11.6				8.6	7.7	11.6	5.9	8.4		
Fossil	3.8	13.4	8.9	8.9	5.4	3.5									6.8	11.0
Agriwaste	16.0	20.4	16.8	22.3	16.1	15.6									13.4	29.1
Other	6.9	15.2	9.0	12.0	6.5	6.7										
Soil	-5.6	/	-9.2	-12.1	-4.7	/										
Eurasia, temperate																
Wetland	3.5	-1.3	1.8	0.9	13.3	2.9	1.7	1.7	1.8							
Biomass Burning	0.9	0.1	0.1	0.5	0.0	0.9				0.5	0.3	0.7	0.6	0.5		
Fossil	14.6	14.1	11.1	16.5	14.5	12.1									12.6	17.9
Agriwaste	12.3	13.3	14.8	13.9	11.6	14.8									14.6	16.1
Other	1.2	3.3	1.2	1.5	1.6	1.2										
Soil	-2.0	/	-2.8	-2.7	-1.7	/										
Eurasia, boreal																
Wetland	12.5	9.1	12.2	10.6	13.9	22.9	4.4	12.8	9.3							
Biomass Burning	1.3	0.9	0.9	1.0	1.3	1.0				1.5	0.7	1.8	1.5	1.7		
Fossil	10.7	4.6	9.3	3.2	3.6	9.7									5.9	16.8
Agriwaste	2.8	1.6	1.9	1.3	1.4	2.5									2.4	6.1
Other	0.7	1.4	0.6	0.8	0.7	0.5										
Soil	-3.9	/	-1.8	-1.4	-4.5	/										
China																
Wetland	4.8	5.0	4.2	2.5	12.4	4.9	6.8	9.9	5.3							
Biomass Burning	3.0	0.1	0.1	1.8	0.2	3.2				4.1	4.2	4.2	4.4	4.1		
Fossil	13.7	17.9	8.6	11.1	20.5	16.0									13.4	10.1
Agriwaste	27.4	28.0	36.3	26.5	21.3	33.7									30.9	25.2
Other	1.2	1.5	0.9	0.6	1.2	1.3										

Soil	-2.0	/	-2.0	-1.2	-1.5	/										
India																
Wetland	1.4	4.0	0.2	4.0	1.9	0.2	16.3	5.2	6.0							
Biomass Burning	2.8	0.3	0.1	1.6	0.1	3.0				1.8	1.7	2.3	2.2	1.8		
Fossil	1.8	4.3	1.6	2.1	1.8	2.0									1.9	3.1
Agriwaste	26.0	22.2	42.6	19.1	22.7	30.0									20.5	24.2
Other	0.8	1.3	0.8	0.7	0.7	0.8										
Soil	-0.6	/	-1.1	-0.8	-0.3	/										
Australia																
Wetland	1.1	-0.4	11.2	1.2	0.5	4.0	3.3	2.7	2.6							
Biomass Burning	0.5	0.1	0.6	0.3	0.5	1.0				0.7	0.9	1.9	0.2	0.8		
Fossil	0.4	0.6	1.6	0.5	1.5	1.4									1.1	1.2
Agriwaste	2.9	2.3	3.1	2.0	3.3	4.5									4.4	5.6
Other	1.3	1.5	1.3	1.4	1.7	1.4										
Soil	-1.7	/	-3.2	-2.7	-1.1	/										
South East Asia																
Wetland	21.9	7.1	32.0	21.9	13.3	16.4	36.6	14.4	27.5							
Biomass Burning	4.9	3.3	3.1	3.1	2.6	5.6				6.3	4.8	2.1	4.8	6.6		
Fossil	3.3	6.4	4.5	2.9	1.8	3.5									3.2	4.6
Agriwaste	14.5	19.9	31.9	15.6	9.5	15.0									18.9	23.8
Other	1.3	3.8	1.8	1.8	1.5	1.2										
Soil	-0.6	/	-2.1	-1.4	-0.3	/										

II Observations and model descriptions

II.1 Description of atmospheric CH_4 datasets

NOAA/ESRL (Dlugokencky et al., 2011)

NOAA air samples are collected in pairs, approximately weekly, in 2.5 L borosilicate-glass flasks with Teflon O-ring sealed stopcocks from sites in NOAA's global cooperative air sampling network[83]. Flasks are flushed and pressurized to ~1.2 atm with a portable sampler. Methane is measured by gas chromatography with flame ionization detection against the NOAA 2004 CH_4 standard scale (it is also the WMO Global Atmosphere Watch CH_4 mole fraction scale)[84] and reported in dry air mole fractions (nmol mol^{-1}, abbreviated ppb). Repeatability of the measurements averages 1.5 ppb (1 s.d.). For this study, measurements from 46 globally-distributed remote boundary layer sites were fitted with curves to smooth variability with periods less than ~40 days[83]. Synchronized points were extracted from these curves at approximately weekly intervals and smoothed as a function of latitude to define an evenly spaced matrix of surface CH_4 mole fractions as a function of time and latitude (data path: ftp://ftp.cmdl.noaa.gov/ccg/ch4/flask/). This matrix was used to calculate global CH_4 averages.

AGAGE (Rigby et al., 2008)

Global-average GAGE/AGAGE CH_4 mole fractions

GAGE CH_4 measurements began between 1985 and 1987 at Adrigole, Ireland, Cape Grim, Tasmania, Cape Mears, Oregon and Cape Matatula, Samoa[2]. These observations have been ongoing throughout the GAGE and subsequent AGAGE project, but with a relocation of the Adrigole (Ireland) and Cape Matatula (California) sites to Mace Head (Ireland) and Trinidad Head (California) respectively, and the addition of CH_4 measurements to the ALE/GAGE/AGAGE site at Ragged Point (Barbados) in 1996. These locations were chosen to sample the remote atmosphere in four "semi-hemispheres". Measurements are made using automated gas chromatograph/flame ionization detectors (GC/FID) at approximately hourly frequency. "Background" concentrations were extracted from the high-frequency measurement time series at each site using a statistical filter[85]. In order to account for data gaps, global average CH_4 mole fractions were calculated using a 2D model of the atmosphere [86,87,88], into which AGAGE observations had been assimilated. CH_4 emissions were estimated in the model in each semi-hemisphere during each month between 1986 and 2011, using AGAGE observations[37]. The global averages were then calculated based on the optimized semi-hemispheric model mole fractions.

CSIRO (Francey et al., 1999)

Sampling:

The CSIRO data used in this manuscript have been obtained from flask air samples returned to GASLAB for analysis. The flasks are of 6 types, 4 of which are the property of CSIRO (items a-d below) and 2 of which are the property of Environment Canada for air sampling at the Canadian sites, Alert and Estevan Point (items e and f): (a) glass 0.5 litre, sealed with two stopcocks fitted with PTFE, PFA or Viton O-rings (flask identifier prefix “G050”), (b) glass 5.0 litre, sealed with two stopcocks fitted with PTFE O-rings (“G500”), (c) glass 0.8 litre, sealed with two stopcocks fitted with PTFE or PFA O-rings (“G080”), (d) electropolished stainless steel 1.6 litre “Sirocans” fitted with two stainless steel valves manufactured by either Nupro or Hoke (“S160”), (e) glass 2.0 litre sealed with a single stopcock fitted with a Viton O-ring (“F”, “FF”, “FA”, “FE”, “EP”, “ALT”) or (f) glass 2.0 litre sealed with two stopcocks fitted with Viton O-rings (“M1”, “S”, “P2”, “TEMP”). Experiments carried out to test for any change in sample CH_4 mixing ratio during storage have shown no drift to within detection limits over test periods of several months to years[89]. Typical sample storage times range from days to weeks for some sites (e.g. Cape Grim, Aircraft) to as much as 1 year for Macquarie Island and the Antarctic sites.

The CSIRO sampling sites used in this study are: South Pole, Antarctica (89° 59’S, 24° 48’W, 2810 metres altitude); Mawson, Australian Antarctic Territory (67° 37’S, 62° 52’E, 32 m); Macquarie Island, Australia (54° 29’S, 158° 58’E, 12 m); Cape Grim, Australia (40° 41’S, 144° 41’E, 94 m);

Cape Ferguson, Australia (19° 17’S, 147° 03’E, 2 m); Mauna Loa, Hawaii, USA (19° 32’N, 155° 35’W, 3397 m); Estevan Point, Canada (49° 23’N, 126° 32’W, 39 m); Shetland, Scotland (60° 10’N, 01° 10’W, 30 m); and Alert, Canada (82° 27’N, 62° 31’W, 6 m).

Analysis:

Samples were analysed by gas chromatography with flame ionisation detection (FID). Three individual but similarly configured Carle gas chromatographs were used over the length of the record. Further details are provided elsewhere of CSIRO’s global sampling network, sampling and analytical techniques[26] and measurement uncertainty[90].

Calibration:

Data are reported in the NOAA04 CH_4scale[84]. The link to this scale was established with 8 high pressure cylinders containing dry, natural air with a CH_4 mole fraction range of 690 - 1870 ppb. These standards were calibrated by NOAA on one or more occasions between 1987 and 2001. Stability of the CSIRO scale is monitored with ~25 assorted long-lived standards. Instrument response has been further evaluated with a suite of six Nippon Sanso CH_4-in-air standards (volumetrically prepared, calibrated against a gravimetric scale at Tohoku University) spanning the range 310-1845 ppb. Details of calibration and measurement uncertainty are given by ref([90]).

Data Processing:

Flask data are assigned flags to indicate whether they are classified as retained or rejected. Cause of rejection falls into three broad categories: (i) the sample is considered to be not representative of the atmosphere at the time and place of sampling due to identified or inferred sampling or analytical problems (eg. sample contamination, poor analysis), (ii) the sample is considered to be “non-baseline” as indicated by the meteorological conditions at the time of sampling and (iii) any remaining outliers are flagged on the basis of a 3 sigma filter. Only data marked as retained have been used in this manuscript.

UCI (Simpson et al., 2012)

The University of California, Irvine (UCI) has monitored global CH_4 mixing ratios since 1978[1 ,27,91 ,92]. Each season (March, June, September, December) more than 80 whole air samples are collected over a 3-week period in a latitudinal transect of the Pacific Basin from 71ºN (Barrow, AK) to 47ºS (Slope Point, New Zealand), with occasional sampling at more northerly and southerly latitudes. Individual air samples are collected at sites that our experience has shown to give remote concentrations, usually along the coast when the wind is arriving from the ocean. A map of the sampling locations for the UCI network is given in ref([27]). Each air sample is collected into a conditioned, evacuated 2 L stainless steel canister equipped with a bellows valve, over a period of about one minute. The air samples are returned to our UCI laboratory and analyzed for CH_4 using gas chromatography (HP-5890A) with flame ionization detection. Other light hydrocarbons and halocarbons are measured from the same air samples using multi-column gas chromatography. Primary CH_4 calibration standards dating back to late 1977 ensure that our measurements are internally consistent. The CH_4 mixing ratios are reported for dry air and are relative to a primary standard purchased from the Matheson Gas Company in 1977, and to a National Bureau of Standards standard that was purchased in 1982 and has an uncertainty of ±1% (comparison with a NIST standard), which is our measurement accuracy. Systematic offsets between networks are regularly quantified and can be corrected when using several international networks in a modelling work. Our analytical precision, which is determined by alternating measurements of secondary standards with aliquots from an individual air sample, is currently about 1 ppbv.

Each data point is individually inspected, and those that do not represent remote values are removed from the data set (typically 2−5 samples per season). The remaining samples are used to calculate a global trace gas mixing ratio for each season of measurements as follows. The earth is divided into 16 latitudinal bands, each with an equal volume of air. The mixing ratios measured in each latitudinal band are averaged, and the global CH_4 mixing ratio for each season is the mean of the 16 band averages. Its uncertainty is the sum of standard errors for each band, added in quadrature, divided by

16. Because we do not routinely collect air samples in the southernmost two latitudinal bands, their CH_4 concentrations are inferred from concentrations measured in neighbouring bands in the southern hemisphere, where CH_4 is well-mixed. The annual global CH_4 mixing ratio is the average of 4 consecutive seasonal means, and its uncertainty is the sum of the standard errors of the seasonal means, added in quadrature, divided by 4. The annual global growth rate is the difference between two consecutive annual global CH_4 mixing ratios. Its uncertainty is the sum of the standard errors of the two annual means from which it was calculated, added in quadrature.

II.2 Description of top-down inversions (T-D)

Model main characteristics are summarized in table S1.

TM5-4DVAR (Bergamaschi et al., 2009)

Model simulations are based on the TM5-4DVAR inverse modelling system described in detail by Meirink[93], including subsequent further developments described by Bergamaschi et al. (2009; 2010)[23,94]. TM5 is an offline transport model[95] , driven by the meteorological fields from the ERA-INTERIM reanalysis. We employ the standard TM5 version (TM5 cycle 1), with 25 vertical layers, and apply a horizontal resolution of 6°x4°. The 4-dimensional variational (4DVAR) optimization technique minimizes iteratively a cost function taking into account an a priori estimate of the emissions, based on the emission inventories used by Bergamaschi et al. (2010)[94]. Column-averaged CH_4 mixing ratios from the Scanning Imaging Absorption Spectrometer for Atmospheric Cartography (SCIAMACHY) instrument[18] onboard ENVISAT are assimilated together with surface observations from the NOAA Earth System Research Laboratory (ESRL) global cooperative air sampling[3], which serve as 'anchor-points' to correct for biases in the satellite retrievals[23] . The CH_4 inversions used in this paper are from the CH_4 re-analysis over the period 2003-2010 in the framework of the Monitoring Atmospheric Composition and Climate (MACC) project http://www.gmes-atmosphere.eu/.

LMDZ-MIOP (Bousquet et al., 2011)

The LMDZ-MIOP inversion model is an analytical inversion that has been used to infer the sources and sinks of carbon dioxide[96,97], methyl-chloroform[98] CH_3CCl_3, and recently di-hydrogen[99] H_2. Briefly, it solves for monthly surface CH_4 emissions for the different categories of sources and sinks and for 11 large regions (10 land regions + 1 ocean), as described in the TRANSCOM experiment[100]. It uses monthly mean observations at up to 68 surface stations from the NOAA/ESRL, CSIRO and IPSL/LSCE surface monitoring networks. The offline version LMDZt version 3 of the LMDZ-GCM, nudged to analysed winds[101], is used to model atmospheric transport[102,103]. Prior emissions are taken from inventories[104-106]. The OH 3-dimensional fields are pre-optimized by an inversion of CH_3CCl_3 (MCF) observations as described by Bousquet et al. (2005)[98]. Monthly uncertainties are prescribed for prior CH_4 emissions of ±150% for each region each month, and for CH_4 observations (from ±5 ppb to ±50ppb, with a median of ±10 ppb), with no error correlations. A simple filter is also added in the time domain: changes of the inferred fluxes from one month to the next are limited to ±250% (sources with a seasonal cycle in the prior data) or to ±50% (sources with no seasonal cycle in the prior data) of the prior month-to-month differences, according to previous studies[107,108]. This noise filter avoids the creation of unrealistic large month-to-month flux differences. A more complete description of the method can be found in Bousquet et al. (2005)[98]. We define a reference inversion scenario based on these assumptions, complemented by four additional scenarios varying the number of atmospheric stations (only NOAA/ESRL stations), the OH IAV (OH is maintained constant), the wetland scenario[109], and the noise filter (no noise filter used).

CarbonTracker-CH_4 (Bruhwiler et al., 2012)

The global CH_4 assimilation, CarbonTracker-CH_4, estimates anthropogenic and natural emissions from 2000 through to the end of 2010. Anthropogenic prior emissions are from the EDGAR 3.2FT2000 dataset and were kept constant over the period of the simulation in order to see whether trends in emissions would be captured by the assimilation. Prior wetland emissions were taken from Bergamaschi et al. (2007)[110] and were based on the work by Mathews and Fung (1987)[104]. Natural prior CH_4 sources also included emissions from wildfires using the GFED product[106], as well as the global soil uptake[111]. Smaller prior emissions from the oceans, termites and wild animals were also included. A diagonal prior covariance matrix was assumed with the uncertainty of individual processes taken to be 75% of the magnitude of each source. To produce flux estimates, CarbonTracker-CH_4 uses the ensemble Kalman smoother described by Peters et al. (2005)[112], and the TM5 transport model with driving meteorology from ECMWF. The estimated parameters are multipliers of the prior flux estimates at weekly intervals, aggregated to monthly values. Air samples from 88 sites distributed globally are used to constrain the flux estimates. Most of the sites were located at the surface; however, at a few sites samples were collected from towers. Aircraft observations were not used, but instead retained for evaluation. The model-data mismatch errors are difficult to quantify for each site; however, sites located in the marine boundary layer and deep Southern Hemisphere were given more weight in the assimilation than continental sites that are more difficult to model due to proximity to local sources. More details on CarbonTracker-CH_4 are given by Bruhwiler et al. (2011)[64].

GEOS-Chem (Fraser et al., 2013)

GEOS-Chem is a global 3-D chemical transport model (v8-01-01) driven by v5 of the analyzed meteorological fields from the NASA Global Modeling and Assimilation Office. A comprehensive description and evaluation of the CH_4 simulation is given by ref([65,113]). Here, the model was run at 4x5 resolution with 47 vertical levels. We use prior year-specific emission inventories for anthropogenic activity (EDGAR 3.2 FT[114]), biomass-burning (GFEDv2[106]), and wetlands and rice[115]; and climatological seasonal emissions for the ocean[116] and all other natural emissions and the soil sink (Fung et al, 1991). We use monthly-mean 3-D fields for the tropospheric OH sink generated from the Ox-NOx-VOC chemistry version of GEOS-Chem[117]. Stratospheric loss rates are adapted from a 2D stratospheric model[118]. We use an ensemble Kalman filter[119] to estimate surface CH_4 fluxes by fitting surface measurements (2000-2010) at 48 sites[108] with measurement errors described by Wang et al. (2004)[118]. We estimate fluxes on an 8-day time step, using a 3.5 month lag window, over 110 regions defined by subdividing each of the 23 continental TransCom regions into 9 regions[100]. For regions with significant contribution from both seasonal and constant sources (temperate North America, North Africa, temperate Eurasia, Europe) we estimate seasonal and constant emissions separately, assigning a prior uncertainty of 50% for land-regions with seasonal emissions and 25% for constant emissions. For all other regions we estimate all emissions together, with a prior uncertainty of 50%. We report monthly mean fluxes on the original 23 TransCom regions.

TM5-4DVAR (Beck et al., 2012)

The TM5-4DVAR inversions make use of the global atmospheric transport model TM5[95]. The off-line TM5 model is driven by meteorological fields from the ERA-interim reanalysis from ECMWF at a resolution 6x4 degree (lat x long) and 25 hybrid sigma pressure levels. The optimization algorithm is based on the variational approach, and uses the conjugate gradients technique for cost function minimization[93]. The inversion solves for net monthly CH_4 fluxes at the resolution of the transport model for the period 2003-2010. A priori emissions are taken from the EDGAR4.1 emission inventory (http://edgar.jrc.ec.europa.eu) for anthropogenic fluxes, LPJ-WhyMe[62] for natural wetlands, and GFED3[34] for biomass-burning, complemented by minor sources[13]. The photochemical removal of CH_4 is calculated using an MCF calibrated OH climatology[29] and accounts for oxidation by Cl and O^{1D} radicals in the stratosphere[120]. TM5-4DVAR optimizes CH_4 surface fluxes to minimize the misfit with measurements of the CH_4 dry air mole fraction from 46 sites of the NOAA-ESRL cooperative flask sampling network[3] and retrievals of vertical column averaged CH_4 from the SCIAMACHY satellite instrument[18] for the period 2003-2010. Posterior flux estimates per source category are derived from the optimized grid box totals using the a priori assumed partitioning between the processes per grid box.

LMDZt-SACS (Pison et al., 2009; Bousquet et al., 2011)

We use the variational scheme[121] including the off-line version of the LMDZt (Laboratoire de Météorologie Dynamique – Zoom) transport model version 4 coupled with the atmospheric chemistry module SACS (Simplified Atmospheric Chemistry System)[122]. LMDz's grid is 3.75 degrees x 2.5

degrees (longitude-latitude) on 19 sigma-pressure levels. The air mass fluxes are pre-computed by the on-line LMDz version nudged to ECMWF analysis for horizontal winds. SACS represents a simplified CH_4 oxidation chain that links CH_4 and CO through reactions with hydroxyl radicals (OH) and formaldehyde (HCHO)[122]; the reaction between OH and methyl-chloroform (MCF, CH_3CCl_3) is also represented as a constraint on OH concentrations. Methane prior inventories are combined from the Emission Database for Global Atmospheric Research (EDGAR~3) inventory for the year 1995[105] for anthropogenic emissions, the Global Fire and Emission database (GFED-v2)[106] for monthly biomass-burning emissions, the study by Fung et al. (1991)[123] for emissions due to wetlands and termites, and a constant source (total 15 Tg/year) for oceans. MCF emissions are based on the inventory of Montzka et al. (2000)[124], rescaled according to an update of the study by Bousquet et al. (2006)[10]. The prior variances in each grid cell are set at ±100% of the monthly maximum flux over the eight neighbouring grid cells and the current grid cell[122]). The error correlations of the CH_4 fluxes are optimized using correlation lengths of 500 km on land and 1000 km on oceans, without time correlations[121]. Daily mean CH_4 and MCF observations at continuous measurement stations and individual flask observations at flask stations are assimilated at 66 surface stations from the NOAA/ESRL, CSIRO and IPSL/LSCE surface monitoring networks. The inversion is run from January 1990 to March 2009. The relevant cost function and the norm of its gradient (computed by the adjoint) are minimized with the algorithm M1QN3[125]. The inversion results consist of eight-day maps (7081 cells) of net CH_4 emission fluxes and four correction coefficients for OH columns (one per latitudinal band 90S-30S; 30S-0, 0-30N, 30N-90N). To compare our results with the other inventories, the total net fluxes are broken into categories. The global monthly analysis-to-prior ratio is computed and then applied to each source category used in the prior in each grid cell over the month.

MATCH model (Chen & Prinn, 2006)

See Table S1

TM2 model (Hein et al., 1997)

See Table S1

GISS model (Fung et al. 1991)

See Table S1

II.3 Description of bottom-up studies (B-U)

LPJ-wsl (Hodson et al, 2011)

The LPJ-wsl CH_4 model output used in this analysis is the same as presented by Hodson et al., (2011)[63]. The wetland CH_4 flux E (Tg CH_4 grid cell^{-1} month^{-1}) at each 0.5° grid cell (x) and monthly time step (t) is calculated as a linear function of wetland extent (A) and heterotrophic respiration (R_h) according to the following equation:

$$E(x,t) = R_h(x,t)A(x,t)\beta F(x) \qquad (1)$$

R_h is calculated using the LPJ-wsl dynamic global vegetation model (DGVM), based on the LPJv3.1 DGVM[126,127]. The monthly climatology inputs (precipitation, mean temperature, cloud cover, wet days) and the non-gridded annual CO_2 concentration inputs to LPJ-wsl are described by Hodson et al. (2011). In addition, we prescribed[63] soil texture from the Food and Agriculture Organization[128], using a 2-soil layer hydrological model with a total soil depth of 1.5 metres. A 1000-year spin up was implemented by recycling the first 30 years of climate data (1901-1930) with pre-industrial CO_2 concentrations to equilibrate soil and vegetation carbon pools, followed by a transient simulation running from 1901-2005.

Wetland extent (A) represents natural wetland area and lakes only and is a monthly-varying combined model and satellite product at 0.5° x 0.5° spatial resolution[63].

The scaling ratio βF converts C to CH_4 fluxes and is a combination of two scaling factors, one for tropical (TR) and one for boreal (B) wetland conditions, which allows the model to account for broad ecosystem differences in CH_4 emitting capacity between wetland types (Eqn. 2). The fraction of wetland type found in each grid cell is calculated based on surface temperature (Eqn. 3).

$$\beta F = \sigma F_{TR} + (1- \sigma)F_B \qquad (2)$$

$$\sigma = \exp((T(x) - T_{max})/8) \qquad (3)$$

where T is the mean near-surface temperature between 1960–1990, and T_{max} = 303.35 K. F_{TR} and F_B were fit to match regional estimates of wetland CH_4 fluxes for the Hudson Bay lowlands and the central Amazon Basin as described by Hodson et al. (2011).

ORCHIDEE (Ringeval et al., 2011)

The ORCHIDEE model[129] has been implemented with a wetland CH_4 emissions scheme. Such an ORCHIDEE version has been used for various studies on different time-scales[61,130]. The model explicitly represents both the mechanisms leading to CH_4 flux at the atmosphere/soil interface and the dynamic wetland extent. Basically, the wetland CH_4 emissions $E_{CH4}(g,t)$ are computed in ORCHIDEE-WET for each grid-cell *g* and for each time-step *t* through the following equation:

$$E_{CH4}(g,t)=\Sigma_{WTDi}(S_{WTDi}(g,t).D_{WTDi}(g,t))$$

Where S_{WTDi} is the fraction of *g* covered by a wetland where the water table depth is equal to WTD_i and D_{WTDi} is the CH_4 flux density (i.e. g CH_4 per m^2 per unit time) for a wetland where the water table depth is equal to WTD_i. Here, the WTD_i values for each grid-cell are taken as: 0, -3 and -6cm. S_{WTDi} and D_{WTDi} are respectively computed by (i) the coupling between a TOPMODEL approach and ORCHIDEE[131] and (ii) the coupling between a slight modification of the Walter model [132] and ORCHIDEE[130]. As in a previous version[61], the wetland extent is corrected to subtract the systematic biases of the model using a mean climatology of the remote sensing data of inundation extent[133]. Moreover, in the present study, two ORCHIDEE estimates are given in which the seasonal cycle of the wetland extent is either prescribed (ORCHIDEE-P07) or computed (ORCHIDEE-TOP). In both estimates, the IAV of the wetland extent is computed.

LPJ-WhyMe (Spahni et al., 2011)

Global CH_4 emissions and sinks have been estimated with the B-U approach using the LPJ-WhyMe dynamic global vegetation model[62]. The model was forced by the CRU-NCEP climate data set[134] and run over the period of 1990-2009. The model runs were performed for four wetland source types of atmospheric CH_4 (northern high latitude peatlands, tropical and subtropical inundated wetlands, global rice paddies and global wet mineral soils) and the global CH_4 soil sink. For peatlands, inundated wetlands and rice paddies the fractional emission area was prescribed according to IGBP-DIS soil carbon map (Global Soil Data Task Group, 2000), inundation map[135], and fractional rice cover map[136], respectively. Areas were treated to be conformal (Spahni et al., 2011) and the non-inundated fractional area of mineral soils could be a CH_4 source or a sink depending on soil moisture content as calculated by the LPJ-WhyMe hydrology[62]. CH_4 emission fluxes per unit area were calculated as being proportional to the model's soil carbon respiration, differentially for each emission and sink type. The global scaling parameters were calibrated by a T-D optimization of the global budget using the TM5 atmospheric chemistry and transport model on the basis of monthly fluxes in 2004[62].

GICC (Mieville et al., 2010)

The Global Inventory for Chemistry-Climate studies (GICC)[69] gridded decadal (for the 1980s and 1990s) and yearly (1997-2005) biomass burning emission fields were downloaded from the ECCAD portal (http://eccad.sedoo.fr, date of access: 14 November, 2011).

RETRO (Schultz et al., 2007)

Yearly gridded emission data sets from the Reanalysis of the TROpospheric chemical composition over the last 40 years project (RETRO)[67] for the period 1980-2000 were downloaded from ftp://ftp.retro.enes.org/pub/emissions/ch4/.

GFEDv2 (Van der Werf et al., 2004)

The Global Fire Emission Database version 2 (GFEDv2)[68] gridded monthly biomass burning emission fields for the period 1997-2008 were downloaded from the ECCAD portal (http://eccad.sedoo.fr, date of access: 30 January, 2012).

GFEDv3 (Van der Werf et al., 2010)

The Global Fire Emission Database version 3 (GFEDv3)[34] gridded monthly biomass burning emission fields for the period 1997-2009 were downloaded from http://www.falw.vu/~gwerf/GFED/GFED3/emissions/ (date of access: 20 July 2011).

FINNv1 (Wiedinmyer et al., 2011)

The Fire Inventory from NCAR (FINNv1)[70] gridded emission fields were gathered by Christine Wiedinmyer and downloaded from the ftp server (date of access: 3 January 2012).

IIASA (Dentener et al., 2005)

IIASA CH_4 data for the 1990's and 2000s and the fossil fuel, agriculture/waste and biomass burning categories[137] were downloaded from http://www.iiasa.ac.at/rains/global_emiss/global_emiss.html (date of access: 7 November 2011).

EPA, 2011

EPA[138,139] CH_4 data for the 1990's and 2000s and the fossil fuel and agriculture/waste categories were downloaded from http://www.epa.gov/climatechange/economics/downloads/Data%20Annexes%20-%202012.zip (date of access: 14 November 2011).

EDGARv4.1 (EDGAR4.1, 2009)

EDGARv4.1[140] gridded emission fields for anthropogenic fluxes were downloaded from the EDGAR website (http://edgar.jrc.ec.europa.eu/datasets_grid_list41.php#, date of access: 26 August, 2011).

EDGARv4.2 (EDGAR4.2, 2011)

EDGARv4.2[140] gridded emission fields for anthropogenic fluxes were downloaded from the EDGAR website (http://edgar.jrc.ec.europa.eu/datasets_list.php?v=42&edgar_compound=CH4, date of access: 20, November 2012).

Description of models contributing to the Atmospheric Chemistry and Climate Model Intercomparison Project (ACCMIP, Lamarque et al., 2013; Voulgarakis et al., 2013; Naik et al., 2013)

The Atmospheric Chemistry and Climate Model Intercomparison Project (ACCMIP)[141,142,152] (http://www.giss.nasa.gov/projects/accmip/) consists of a series of timeslice experiments targeting the long-term changes in atmospheric composition between 1850 and 2100, with the goal of documenting radiative forcing and the associated composition changes. Methane chemical destruction due to OH from 9 of the 12 ACCMIP models is included in this study. All the models are run as coupled chemistry-climate models (CCMs), driven by monthly mean sea-surface temperatures and sea-ice coverage either from observations or from the corresponding coupled ocean-atmosphere model integrations submitted to the Coupled Model Intercomparison Project Phase 5 (CMIP5). All details about model specifications and performed simulations can be found in the related publications[142,143].

In most models, CH_4 concentration was prescribed at the surface using the historical reconstruction but was allowed to undergo chemical processing in the rest of the atmosphere. In LMDzORINCA surface CH_4 emissions were specified following ref([144]), while UM-CAM used a globally constant concentration. In all models, CH_4 varies between different timeslices. Ozone photolysis is the primary source of hydroxyl radicals (OH), the main sink for CH_4, in the troposphere. CESM-CAM-superfast, CMAM, GFDL-AM3[145], LMDzORINCA, MIROC-CHEM, NCAR-CAM3.5, and UM-CAM employed a lookup table approach wherein calculated clear-sky photolysis frequencies are adjusted for modelled clouds, overhead ozone column, and surface albedo. The GEOSCCM, and GISS-E2-R models used versions of the Fast-J scheme[146], which calculates photolysis frequencies online accounting for modelled clouds, overhead ozone column, surface albedo and aerosols. Overhead stratospheric ozone column determines the level of incoming ultraviolet radiation, important for the formation of tropospheric OH radicals. Six of the nine models simulated full stratospheric chemistry. Stratospheric ozone concentrations in the UM-CAM and LMDzORINCA were prescribed from a database[147] developed in support of CMIP5 and a climatology[148], respectively. In CESM-CAM-superfast, a simplified “linearized ozone chemistry” (LINOZ) scheme was used.

We used data from the 1980 and 2000 timeslices simulated within the ACCMIP intercomparison, representing the CH_4 chemical loss for the years around 1980 and 2000. This provides estimates of CH_4 loss due to OH for the 1980s and the 2000s, two of the decades we are interested in. Only two of the models, LMDzORINCA and GISS-E2-R, provided a full year-to-year dataset from transient simulations for all three decades. Since no model simulated a 1990 timeslice, we only used those two models to estimate CH_4 chemical loss for the 1990s. This explains why we get fewer estimates in the 1990s than in the 1980s and the 2000s (Fig. 2).

TM5 full chemistry model (Williams et al., 2012; Huijnen et al., 2010)

Forward simulations using the TM5 chemistry-transport model in full chemistry mode and relaxation to CH_4 surface concentrations provide information on the global sink term. Information on CH_4 emissions is obtained following a semi-inverse approach[149]. Forward simulations using TM5 and including CH_4 emissions[62] and latest anthropogenic emission inventories[140] provide information on the 3D time evolution of the OH field. The full chemistry simulations are performed on 3x2 degrees (longitude x latitude) grid and 34 sigma-pressure vertical levels. The calculated CH_4 losses for the years 2000-2009 are given for the TM5 model version referenced in refs ([150,151]).

III References

1 Blake, D. R. *et al.* Global Increase in Atmospheric Methane Concentrations between 1978 and 1980. *Geophys. Res. Lett.* **9**, 477-480 (1982).

2 Cunnold, D. M. *et al.* In situ measurements of atmospheric methane at GAGE/AGAGE sites during 1985-2000 and resulting source inferences. *J. Geophys. Res.-atmos.* **107**, ACH 20-21-ACH 20-18, doi:10.1029/2001jd001226 (2002).

3 Dlugokencky, E. J. *et al.* Observational constraints on recent increases in the atmospheric CH burden, . *Geophys. Res. Lett.*, **36**, L18803, doi:doi:10.1029/2009GL039780. (2009).

4 Francey, R. J. *et al.* Atmospheric carbon dioxide and its stable isotope ratios, methane, carbon monoxide, nitrous oxide and hydrogen from Shetland Isles. *Atmos. Environ.* **32**, 3331-3338 (1998).

5 Brenninkmeijer, C. A. M. *et al.* Civil Aircraft for the regular investigation of the atmosphere based on an instrumented container: The new CARIBIC system. *Atmos. Chem. Phys.* **7**, 4953-4976, doi:10.5194/acp-7-4953-2007 (2007).

6 Wecht, K. J. *et al.* Validation of TES methane with HIPPO aircraft observations: implications for inverse modeling of methane sources. *Atmos. Chem. Phys.* **12**, 1823-1832, doi:10.5194/acp-12-1823-2012 (2012).

7 WMO. *WMO World Data Centre for Greenhouse Gases*, <http://ds.data.jma.go.jp/gmd/wdcgg/introduction.html> (2012).

8 Sussmann, R., Forster, F., Rettinger, M. & Bousquet, P. Renewed methane increase for five years (2007,Äì2011) observed by solar FTIR spectrometry. *Atmos. Chem. Phys.* **12**, 4885-4891, doi:10.5194/acp-12-4885-2012 (2012).

9 Wunch, D. *et al.* The Total Carbon Column Observing Network, . *Phil. Trans. R. Soc. A*, **369**, doi: 10.1098/rsta.2010.0240 (2011).

10 Bousquet, P. *et al.* Contribution of anthropogenic and natural sources to atmospheric methane variability. *Nature* **443**, 439-443 (2006).

11 Fisher, R. E. *et al.* Arctic methane sources: Isotopic evidence for atmospheric inputs. *Geophys. Res. Lett.* **38**, L21803, doi:10.1029/2011gl049319 (2011).

12 Mikaloff Fletcher, S. E. M., Tans, P. P., Bruhwiler, L. M., Miller, J. B. & Heimann, M. CH4 sources estimated from atmospheric observations of CH4 and its C-13/C-12 isotopic ratios: 1. Inverse modeling of source processes. *Global. Biogeochem. Cycles* **18**, GB4004, doi:4010.1029/2004GB002223 (2004).

13 Monteil, G. *et al.* Interpreting methane variations in the past two decades using measurements of CH(4) mixing ratio and isotopic composition. *Atmos Chem Phys* **11**, 9141-9153 (2011).

14 Neef, L., van Weele, M. & van Velthoven, P. Optimal estimation of the present-day global methane budget. *Global. Biogeochem. Cycles* **24** (2010).

15 Wahlen, M. The Global Methane Cycle. *Annual Review of Earth and Planetary Sciences* **21**, 407-426, doi:doi:10.1146/annurev.ea.21.050193.002203 (1993).

16 Lassey, K. R., Lowe, D. C. & Smith, A. M. The atmospheric cycling of radiomethane and the "fossil fraction" of the methane source. *Atmos Chem Phys* **7**, 2141-2149 (2007).

17 Crevoisier, C. *et al.* First year of upper tropospheric integrated content of CO(2) from IASI hyperspectral infrared observations. *Atmos Chem Phys* **9**, 4797-4810 (2009).

18 Frankenberg, C. *et al.* Global column-averaged methane mixing ratios from 2003 to 2009 as derived from SCIAMACHY: Trends and variability. *J. Geophys. Res.-atmos.* **116**, D04302, doi:10.1029/2010jd014849 (2011).

19 Morino, I. *et al.* Preliminary validation of column-averaged volume mixing ratios of carbon dioxide and methane retrieved from GOSAT short-wavelength infrared spectra. *Atmos Meas Tech* **4**, 1061-1076 (2011).

20 Butz, A. *et al.* Toward accurate CO(2) and CH(4) observations from GOSAT. *Geophys. Res. Lett.* **38**, L14812, doi:10.1029/2011gl047888 (2011).

21 Parker, R. *et al.* Methane observations from the Greenhouse Gases Observing SATellite: Comparison to ground-based TCCON data and model calculations. *Geophys. Res. Lett.* **38**, L15807, doi:10.1029/2011gl047871 (2011).

22 Frankenberg, C. *et al.* Satellite chartography of atmospheric methane from SCIAMACHY on board ENVISAT: Analysis of the years 2003 and 2004. *J. Geophys. Res.-atmos.* **111**, D07303, doi:DOI: 10.1029/2005JD006235 (2006).

23 Bergamaschi, P. *et al.* Inverse modeling of global and regional CH4 emissions using SCIAMACHY satellite retrievals. *J. Geophys. Res.-atmos.* **114**, doi:10.1029/2009JD012287 (2009).

24 Dlugokencky, E. J., Nisbet, E. G., Fisher, R. & Lowry, D. Global atmospheric methane: budget, changes and dangers. *Philos T R Soc A* **369**, 2058-2072 (2011).

25 Rigby, M. *et al.* Renewed growth of atmospheric methane. *Geophys. Res. Lett.* **35**, **-** (2008).

26 Francey, R. J., Steele, L. P., Langenfelds, R. L. & Pak, B. C. High precision long-term monitoring of radiatively active and related trace gases at surface sites and from aircraft in the southern hemisphere atmosphere. *J Atmos Sci* **56**, 279-285 (1999).

27 Simpson, I. J. *et al.* Long-term decline of global atmospheric ethane concentrations and implications for methane. *Nature* **488**, 490-494, doi:http://www.nature.com/nature/journal/v488/n7412/abs/nature11342.html (2012).

28 Thoning, K. W., Tans, P. P. & Komhyr, W. D. Atmospheric carbon dioxide at Mauna Loa Observatory. 2. Analysis of the NOAA GMCC data, 1974,1985. *J. Geophys. Res.* **94**, 8549-8565 (1989).

29 Montzka, S. A. *et al.* Small Interannual Variability of Global Atmospheric Hydroxyl. *Science* **331**, 67-69 (2011).

30 Dlugokencky, E. J. *et al.* Changes in CH4 and CO growth rates after the eruption of Mt Pinatubo and their link with changes in tropical tropospheric UV flux. *Geophys. Res. Lett.* **23**, 2761-2764 (1996).

31 Chen, Y. H. & Prinn, R. G. Estimation of atmospheric methane emissions between 1996 and 2001 using a three-dimensional global chemical transport model. *J. Geophys. Res.-atmos.* **111**, doi:10.1029/2005JD006058 (2006).

32 Dlugokencky, E. J. *et al.* Atmospheric methane levels off: Temporary pause or a new steady-state? *Geophys. Res. Lett.* **30**, 1992, doi:1910.1029/2003GL018126, doi:ftp://ftp.cmdl.noaa.gov/ccg (2003).

33 Langenfelds, R. L. *et al.* Interannual growth rate variations of atmospheric CO2 and its delta C-13, H-2, CH4, and CO between 1992 and 1999 linked to biomass burning. *Global. Biogeochem. Cycles* **16**, 1048, doi: doi:10.1029/2001GB001466 (2002).

34 van der Werf, G. R. *et al.* Global fire emissions and the contribution of deforestation, savanna, forest, agricultural, and peat fires (1997-2009). *Atmos Chem Phys* **10**, 11707-11735 (2010).

35 Prinn, R. G. *et al.* Evidence for variability of atmospheric hydroxyl radicals over the past quarter century. *Geophys. Res. Lett.* **32**, L07809, doi:07810.01029/02004GL022228 (2005).

36 Bousquet, P. *et al.* Source attribution of the changes in atmospheric methane for 2006-2008. *Atmos Chem Phys* **11**, 3689-3700 (2011).

37 Rigby, M. *et al.* Renewed growth of atmospheric methane. *Geophys. Res. Lett.* **35**, L22805, doi:10.1029/2008gl036037 (2008).

38 Sanderson, M. G. Biomass of termites and their emissions of methane and carbon dioxide: A global database. *Global Biogeochem. Cycles* **10**, 543-557, doi:10.1029/96gb01893 (1996).

39 Sugimoto, A., Inoue, T., Kirtibutr, N. & Abe, T. Methane oxidation by termite mounds estimated by the carbon isotopic composition of methane. *Global Biogeochem. Cycles* **12**, 595-605, doi:10.1029/98gb02266 (1998).

40 Bignell, D. E., Eggleton, P., Nunes, L. & Thomas, K. L. in *Forests and Insects* (ed N.E. Stork and M.D. Hunter (Editors) A.D. Watt) 109-134 (Chapman and Hall, 1997).

41 Jung, M., Reichstein, M. & Bondeau, A. Towards global empirical upscaling of FLUXNET eddy covariance observations: validation of a model tree ensemble approach using a biosphere model. *Biogeosciences* **6**, 2001-2013, doi:10.5194/bg-6-2001-2009 (2009).

42 Jung, M. *et al.* Global patterns of land-atmosphere fluxes of carbon dioxide, latent heat, and sensible heat derived from eddy covariance, satellite, and meteorological observations. *J. Geophys. Res.* **116**, G00J07, doi:10.1029/2010jg001566 (2011).

43 Ramankutty, N. & Foley, J. A. Estimating historical changes in global land cover: Croplands from 1700 to 1992. *Global Biogeochem. Cycles* **13**, 997-1027, doi:10.1029/1999gb900046 (1999).

44 Attignon, S. E., Lachat, T., Sinsin, B., Nagel, P. & Peveling, R. Termite assemblages in a West-African semi-deciduous forest and teak plantations *Agr. Ecosys. Environ.* **110**, 318–326 (2005).

45 Jones, D. T. *et al.* Termite assemblage collapse along a land-use intensification gradient in lowland central Sumatra, Indonesia, . *J. Appl. Ecol.* **40**, 380–391 (2003).

46 Kagezi, G. H. *et al.* Decomposition of tissue baits and termite density along a gradient of human land-use intensification in Western Kenya, Afr. *J. Ecol.* **49**, 267–276 (2011).

47 Rahman, P. M., Varma, R.V., Sileshi, G.W.: . Abundance and diversity of soil invertebrates in annual crops, agroforestry and forest ecosystems in the Nilgiri biosphere reserve of Western Ghats, India, . *Agroforest Syst.* , DOI 10.1007/s10457-10011-19386-10453, doi:DOI 10.1007/s10457-011-9386-3 (2011).

48 Abensperg-Traun, M. & de Boer, E. S. Species abundances and habitat differences in biomass of subterranean termites (isoptera) in the wheatbelt of western Australia. *Aust. J. Ecol.* **15**, 219-226 (1990).

49 Martius, C. *et al.* Methane emission from wood- feeding termites in Amazonia. *Chemosphere* **26**, 623-632 (1993).

50 Macdonald, J. A., Eggleton, P., Bignell, D. E., Forzi, F. & Fowler, D. Methane emission by termites and oxidation by soils, across a forest disturbance gradient in the Mbalmayo Forest Reserve, Cameroon. *Glob. Change Biol.* **4**, 409-418 (1998).

51 Macdonald, J. A. *et al.* The effect of termite biomass and anthropogenic disturbance on the CH4 budgets of tropical forests in Cameroon and Borneo. *Glob. Change Biol.* **5**, 869-879. (1999).

52 Fraser, P. J., Rasmussen, R. A., Creffield, J. W., French, J. R. & Khalil, M. A. K. Termites and global methane – another assessment. *J. Atmos. Chem.,* **4**, 295-310 (1986).

53 Keppler, F., Hamilton, J. T. G., Brass, M. & Rockmann, T. Methane emissions from terrestrial plants under aerobic conditions. *Nature* **439**, 187-191 (2006).

54 Frankenberg, C., Meirink, J. F., van Weele, M., Platt, U. & Wagner, T. Assessing methane emissions from global space-borne observations. *Science* **308**, 1010-1014 (2005).

55 Frankenberg, C. *et al.* Tropical methane emissions: A revised view from SCIAMACHY onboard ENVISAT. *Geophys. Res. Lett.* **35**, L15811, doi:doi:10.1029/2008GL034300 (2008).

56 Dueck, T. A. *et al.* No evidence for substantial aerobic methane emission by terrestrial plants: a 13C-labelling approach,. *New Phytologist* **10.1111/j.1469-8137.2007.02103.x.** (2007).

57 Nisbet, R. E. R. *et al.* Emission of methane from plants. *P Roy Soc B-Biol Sci* **276**, 1347-1354 (2009).

58 Vigano, I. *et al.* Effect of UV radiation and temperature on the emission of methane from plant biomass and structural components. *Biogeosciences* **5**, 937-947 (2008).

59 Bloom, A. A. *et al.* Global methane emission estimates from ultraviolet irradiation of terrestrial plant foliage. *New Phytologist* **doi:10.1111/j.1469-8137.2010.03259.x** (2010).

60 Houweling, S., van der Werf, G. R., Goldewijk, K. K., Rockmann, T. & Aben, I. Early anthropogenic CH4 emissions and the variation of CH4 and (CH4)-C-13 over the last millennium. *Global. Biogeochem. Cycles* **22**, - (2008).

61 Ringeval, B. *et al.* Climate-CH(4) feedback from wetlands and its interaction with the climate-CO(2) feedback. *Biogeosciences* **8**, 2137-2157 (2011).

62 Spahni, R. *et al.* Constraining global methane emissions and uptake by ecosystems. *Biogeosciences* **8**, 1643-1665, doi:10.5194/bg-8-1643-2011 (2011).

63 Hodson, E. L., Poulter, B., Zimmermann, N. E., Prigent, C. & Kaplan, J. O. The El Niño Southern Oscillation and wetland methane interannual variability. *Geophys. Res. Lett.* **38**, L08810, doi:10.1029/2011gl046861 (2011).

64 Bruhwiler, L., Dlugokencky, E. J. & Masarie, K. in *AGU Fall Meeting* Vol. Abstract B11G-01 (San Francisco, Calif., , 2011).

65 Fraser, A. *et al.* Estimating regional methane surface fluxes: the relative importance of surface and GOSAT mole fraction measurements. *Atmos. Chem. Phys.* **13**, 5697-5713, doi:10.5194/acp-13-5697-2013 (2013).

66 Beck, V. *et al.* Methane airborne measurements and comparison to global models during BARCA. *Journal of Geophysical Research: Atmospheres* **117**, D15310, doi:10.1029/2011jd017345 (2012).

67 Schultz, M. G. *et al.* Emission data sets and methodologies for estimating emissions., (Hamburg., 2007).

68 van der Werf, G. R. *et al.* Continental-scale partitioning of fire emissions during the 1997 to 2001 El Nino/La Nina period. *Science* **303**, 73-76 (2004).

69 Mieville, A. *et al.* Emissions of gases and particles from biomass burning during the 20th century using satellite data and an historical reconstruction. *Atmos. Environ.* **44**, 1469-1477, doi:10.1016/j.atmosenv.2010.01.011 (2010).

70 Wiedinmyer, C. *et al.* The Fire INventory from NCAR (FINN): a high resolution global model to estimate the emissions from open burning. *Geosci Model Dev* **4**, 625-641 (2011).

71 Beer, C. *et al.* Terrestrial Gross Carbon Dioxide Uptake: Global Distribution and Covariation with Climate. *Science* **329**, 834-838, doi:10.1126/science.1184984 (2010).

72 Kanniah, K. D., Beringer, J. & Hutley, L. B. Environmental controls on the spatial variability of savanna productivity in the Northern Territory Australia. *Agr. Forest Meteorol.* **151**, 1429– 1439 (2011).

73 Maldague, M. E. in *Trans. 8th Int. Congr. Soil Sci.,* . (eds C. Martius, R. Wassmann, & U. Thein) 743-751.

74 Lepage, M. *Les termites d'une savane sahélienne (Ferlo Septentrional, Sénégal): peuplement, populations, consummation, rôle dans l'écosystème*, Univ. of Djion, , (1974).

75 Ohiagu, C. E. Nest and soil populations of Trinervitermes spp. with particular reference to T. geminatus (Wasmann), (Isoptera), in Southern Guinea savanna near Mokwa, Nigeria, . *Oecologia* **40**, 167-178 (1978).

76 Wood, T. G., Johnson, R. A. & Ohiagu, C. E. Populations of termites (Isoptera) in natural and agriculturalecosystems in Southern Guinea savanna near Mokwa,Nigeria. *Geo. Eco. Trop.* **1**, 139-148 (1977).

77 Abe, T. & Matsumoto, T. Studies on the distribution and ecological role of termites in a lowland rain forest of west Malaysia, 3, Distribution and abundance of termites in Pasoh forest reserve. *Jpn. J. Ecol.* **29**, 337-351 (1979).

78 Ferrar, P. Termites of a south African savanna, I, List of species and subhabitat preferences. *Oecologia* **52**, 125-132 (1982).

79 Ferrar, P. Termites of a south African savanna, IV, Subterranean populations, mass determination and biomass estimations. *Oecologia* **52**, 147-151 (1982).

80 Wood, T. G., Johnson, R. A., Bacchus, S., Shittu, M. O. & Anderson, J. M. Abundance and distribution of termites (Isoptera) in a riparian forest in the Southern Guinea savanna zone of Nigeria. *Biotropica* **14**, 25–39 (1982).

81 Holt, J. A. & Easey, J. F. Numbers and biomass of mound-building termites (isopteran) in a semi-arid tropical woodland near Charters Towers, north Queensland, Australia. *Sociobiolog* **21**, 281-286 (1993).

82 Inoue, T. *et al.* The abundance and biomass of subterranean termites (Isoptera) in a dry evergreen forest of northeast Thailand. *Sociobiology* **37**, 41-52 (2000).

83 Dlugokencky, E. J., Steele, L. P., Lang, P. M. & Masarie, K. A. The Growth-Rate and Distribution of Atmospheric Methane. *J. Geophys. Res.-atmos.* **99**, 17021-17043 (1994).

84 Dlugokencky, E. J. *et al.* Conversion of NOAA atmospheric dry air CH4 mole fractions to a gravimetrically prepared standard scale. *J. Geophys. Res.,* **110**, doi:10.1029/2005JD006035. (2005).

85 O'doherty, S. *et al.* In situ chloroform measurements at Advanced Global Atmospheric Gases Experiment atmospheric research stations from 1994 to 1998. *J. Geophys. Res.-atmos.* **106**, 20429-20444 (2001).

86 Cunnold, D. M. *et al.* The Atmospheric Lifetime Experiment .3. Lifetime Methodology and Application to 3 Years of Cfcl3 Data. *J Geophys Res-Oc Atm* **88**, 8379-8400 (1983).

87 Cunnold, D. M. *et al.* Global Trends and Annual Releases of Ccl3f and Ccl2f2 Estimated from Ale/Gage and Other Measurements from July 1978 to June 1991. *J. Geophys. Res.-atmos.* **99**, 1107-1126 (1994).

88 Rigby, M. *et al.* Re-evaluation of the lifetimes of the major CFCs and CH3CCl3 using atmospheric trends. *Atmos. Chem. Phys.* **13**, 2691-2702, doi:10.5194/acp-13-2691-2013 (2013).

89 Cooper, L. N., Steele, L. P., Langenfelds, R. L., Spencer, D. A. & P., L. M. Atmospheric methane, carbon dioxide, hydrogen, carbon monoxide and nitrous oxide from Cape Grim flask air samples analysed by gas chromatography. . 98pp (Bureau of Meteorology and CSIRO Atmospheric Research, Melbourne, 1999).

90 Francey, R. J. & Steele, L. P. Measuring atmospheric carbon dioxide - the calibration challenge. *Accredit Qual Assur* **8**, 200-204 (2003).

91 Simpson, I. J., Blake, D. R., Rowland, F. S. & Chen, T. Y. Implications of the recent fluctuations in the growth rate of tropospheric methane. *Geophys. Res. Lett.* **29** (2002).

92 Simpson, I. J., Rowland, F. S., Meinardi, S. & Blake, D. R. Influence of biomass burning during recent fluctuations in the slow growth of global tropospheric methane. *Geophys. Res. Lett.* **33** (2006).

93 Meirink, J. F., Bergamaschi, P. & Krol, M. C. Four-dimensional variational data assimilation for inverse modelling of atmospheric methane emissions: method and comparison with synthesis inversion. *Atmos Chem Phys* **8**, 6341-6353 (2008).

94 Bergamaschi, P. *et al.* Inverse modeling of European CH(4) emissions 2001-2006. *J. Geophys. Res.-atmos.* **115** (2010).

95 Krol, M. *et al.* The two-way nested global chemistry-transport zoom model TM5: algorithm and applications. *Atmos Chem Phys* **5**, 417-432 (2005).

96 Peylin, P. *et al.* Multiple constraints on regional CO2 flux variations over land and oceans. *Global. Biogeochem. Cycles* **19**, - (2005).

97 Bousquet, P. *et al.* Regional changes in carbon dioxide fluxes of land and oceans since 1980. *Science* **290**, 1342-1346 (2000).

98 Bousquet, P., Hauglustaine, D. A., Peylin, P., Carouge, C. & Ciais, P. Two decades of OH variability as inferred by an inversion of atmospheric transport and chemistry of methyl chloroform. *Atmos Chem Phys* **5**, 2635-2656 (2005).

99 Bousquet, P. *et al.* A three-dimensional synthesis inversion of the molecular hydrogen cycle: Sources and sinks budget and implications for the soil uptake. *J. Geophys. Res.-atmos.* **116**, **-** (2011).

100 Gurney, K. R. *et al.* Transcom 3 inversion intercomparison: Model mean results for the estimation of seasonal carbon sources and sinks. *Global. Biogeochem. Cycles* **18**, GB2010, doi:10.1029/2003gb002111 (2004).

101 Uppala, S. M. *et al.* The ERA-40 Reanalysis. *J. Roy. Met. Soc.* **131**, 2961-3012 (2005).

102 Hourdin, F. & Talagrand, O. Eulerian backtracking of atmospheric tracers. I: Adjoint derivation and parametrization of subgrid-scale transport. *Quarterly Journal of the Royal Meteorological Society* **132**, 567-583 (2006).

103 Hourdin, F. D., Couvreux, F. & Menut, L. Parameterization of the dry convective boundary layer based on a mass flux representation of thermals. *J Atmos Sci* **59**, 1105-1123 (2002).

104 Matthews, E. & Fung, I. Methane emissions from natural wetlands, global distribution, area and environmental characteristics of sources. *Global. Biogeochem. Cycles* **1**, 61-86 (1987).

105 Olivier, J. G. J. & Berdowski, J. J. M. in *The Climate System,* (eds J. Berdowski, R. Guichert, & B. Heij) p. 33–78 (A.A. Balkema Publishers/Swets & Zeitlinger Publishers, 2001).

106 van der Werf, G. R. *et al.* Interannual variability in global biomass burning emissions from 1997 to 2004. *Atmos Chem Phys* **6**, 3423-3441 (2006).

107 Peylin, P., Bousquet, P., Ciais, P. & Monfray, P. in *Inverse methods in global biogeochemical cycles, Geophysical Monograph 114* (eds P. Kashibata *et al.*) (American Geophysical Union,, 1999).

108 Peylin, P., Baker, D., Sarmiento, J., Ciais, P. & Bousquet, P. Influence of transport uncertainty on annual mean and seasonal inversions of atmospheric CO2 data. *J. Geophys. Res.-atmos.* **107**, 4385, doi:4310.1029/2001JD000857 (2002).

109 Kaplan, J. O. Wetlands at the Last Glacial Maximum: Distribution and methane emissions. *Geophys. Res. Lett.* **29**, 1079, doi:10.1029/2001gl013366 (2002).

110 Bergamaschi, P. *et al.* Satellite chartography of atmospheric methane from SCIAMACHYon board ENVISAT: 2. Evaluation based on inverse model simulations. *J. Geophys. Res.-atmos.* **112**, **-** (2007).

111 Ridgwell, A. J., Marshall, S. J. & Gregson, K. Consumption of atmospheric methane by soils: A process-based model. *Global Biogeochem. Cycles* **13**, 59-70, doi:10.1029/1998gb900004 (1999).

112 Peters, W. *et al.* An ensemble data assimilation system to estimate CO2 surface fluxes from atmospheric trace gas observations. *J. Geophys. Res.-atmos.* **110**, D24304, doi:24310.21029/22005JD006157 (2005).

113 Fraser, A. *et al.* The Australian methane budget: Interpreting surface and train-borne measurements using a chemistry transport model. *Journal of Geophysical Research: Atmospheres* **116**, D20306, doi:10.1029/2011jd015964 (2011).

114 Olivier, J. G. J., van Aardenne, J. A., Dentener, F., Ganzeveld, L. & Peters, J. A. H. W. in *Non‐ CO2 Greenhouse Gases (NCGG‐ 4)*, . (ed A. van Amstel) pp. 325–330, (Millpress, Rotterdam).

115 Bloom, A. A., Palmer, P. I., Fraser, A., Reay, D. S. & Frankenberg, C. Large-Scale Controls of Methanogenesis Inferred from Methane and Gravity Spaceborne Data. *Science* **327**, 322-325, doi:10.1126/science.1175176 (2010).

116 Houweling, S., Kaminski, T., Dentener, F., Lelieveld, J. & Heimann, M. Inverse modeling of methane sources and sinks using the adjoint of a global transport model. *J. Geophys. Res.-atmos.* **104**, 26137-26160 (1999).

117 Fiore, A. *et al.* Variability in surface ozone background over the United States: Implications for air quality policy. *J. Geophys. Res.* **108**, 4787, doi:10.1029/2003jd003855 (2003).

118 Wang, J. S. *et al.* A 3-D model analysis of the slowdown and interannual variability in the methane growth rate from 1988 to 1997. *Global. Biogeochem. Cycles* **18**, 3011, doi:3010.1029/2003GB002180 (2004).

119 Feng, L. *et al.* Evaluating a 3-D transport model of atmospheric CO2 using ground-based, aircraft, and space-borne data. *Atmos. Chem. Phys.* **11**, 2789-2803, doi:10.5194/acp-11-2789-2011 (2011).

120 Law, K. S. & Pyle, J. A. Modeling trace gas budgets in the troposphere: 1. Ozone and odd nitrogen. *Journal of Geophysical Research: Atmospheres* **98**, 18377-18400, doi:10.1029/93jd01479 (1993).

121 Chevallier, F. *et al.* Inferring CO2 sources and sinks from satellite observations: Method and application to TOVS data. *J. Geophys. Res.-atmos.* **110**, doi:D24309
10.1029/2005jd006390 (2005).

122 Pison, I., Bousquet, P., Chevallier, F., Szopa, S. & Hauglustaine, D. Multi-species inversion of CH4, CO and H-2 emissions from surface measurements. *Atmos Chem Phys* **9**, 5281-5297 (2009).

123 Fung, I. *et al.* Three-dimensional model synthesis of global methane cycle. *J. Geophys. Res.* **96**, 13033-13065 (1991).

124 Montzka, S. A. *et al.* New observational constraints for atmospheric hydroxyl on global and hemispheric scales. *Science* **288**, 500-503 (2000).

125 Gilbert, J.-C. & Lemaréchal, C. Some numerical experiments with variable-storage quasi-Newton algorithms. *Mathematical programming* **45**, 407–435. (1989).

126 Sitch, S. *et al.* Evaluation of ecosystem dynamics, plant geography and terrestrial carbon cycling in the LPJ dynamic global vegetation model. *Glob Change Biol* **9**, 161-185 (2003).

127 Gerten, D., Schaphoff, S., Haberlandt, U., Lucht, W. & Sitch, S. Terrestrial vegetation and water balance—hydrological evaluation of a dynamic global vegetation model. *Journal of Hydrology* **286**, 249-270, doi:10.1016/j.jhydrol.2003.09.029 (2004).

128 Zobler, L. A world soil file for global climate modelling. 32 pages. (NASA/GISS, New York USA, 1986).

129 Krinner, G. *et al.* A dynamic global vegetation model for studies of the coupled atmosphere-biosphere system. *Global. Biogeochem. Cycles* **19**, - (2005).

130 Ringeval, B. *et al.* An attempt to quantify the impact of changes in wetland extent on methane emissions on the seasonal and interannual time scales. *Global. Biogeochem. Cycles* **24**, doi:Gb2003 10.1029/2008gb003354 (2010).

131 Ringeval, B. *et al.* Modelling sub-grid wetland in the ORCHIDEE global land surface model: evaluation against river discharges and remotely sensed data. *Geosci. Model Dev.* **5**, 941-962, doi:10.5194/gmd-5-941-2012 (2012).

132 Walter, B. P., Heimann, M. & Matthews, E. Modeling modern methane emissions from natural wetlands 2. Interannual variations 1982-1993. *J. Geophys. Res.-atmos.* **106**, 34207-34219 (2001).

133 Papa, F. *et al.* Interannual variability of surface water extent at the global scale, 1993–2004. *J. Geophys. Res.* **115**, D12111, doi:10.1029/2009jd012674 (2010).

134 Viovy, N. & Ciais, P. Vol. http://dods.extra.cea.fr/data/p529viov/cruncep/readme.htm (2009).

135 Prigent, C., Papa, F., Aires, F., Rossow, W. B. & Matthews, E. Global inundation dynamics inferred from multiple satellite observations, 1993-2000. *J. Geophys. Res.-atmos.* **112**, -, doi:doi:10.1029/2006JD007847 (2007).

136 Leff, B., Ramankutty, N. & Foley, J. A. Geographic distribution of major crops across the world. *Global Biogeochem. Cycles* **18**, GB1009, doi:10.1029/2003gb002108 (2004).

137 Dentener, F. *et al.* The impact of air pollutant and methane emission controls on tropospheric ozone and radiative forcing: CTM calculations for the period 1990-2030. *Atmos Chem Phys* **5**, 1731-1755 (2005).

138 EPA. Global Anthropogenic Non-CO2 Greenhouse Gas Emissions: 1990 - 2030. (U.S. Environmental Protection Agency, Washington, DC 20460, 2011).

139 Environmental Protection Aagency report: Methane and Nitrous Oxide Emissions From Natural Sources. http://www.epa.gov/methane/pdfs/Methane-and-Nitrous-Oxide-Emissions-From-Natural-Sources.pdf, U.S. Environmental Protection Agency, Washington, DC 20460 (2010).

140 European Commission, Joint Research Centre (JRC)/Netherlands Environmental Assessment Agency (PBL). Emission Database for Global Atmospheric Research (EDGAR), release version 4.2. http://edgar.jrc.ec.europa.eu, 2011.

141 Lamarque, J. F. *et al.* The Atmospheric Chemistry and Climate Model Intercomparison Project (ACCMIP): overview and description of models, simulations and climate diagnostics. *Geosci. Model Dev.* **6**, 179-206, doi:10.5194/gmd-6-179-2013 (2013).

142 Voulgarakis, A. *et al.* Analysis of present day and future OH and methane lifetime in the ACCMIP simulations. *Atmos. Chem. Phys.* **13**, 2563-2587, doi:10.5194/acp-13-2563-2013 (2013).

143 Lamarque, J. F. *et al.* The Atmospheric Chemistry and Climate Model Intercomparison Project (ACCMIP): overview and description of models, simulations and climate diagnostics. *Geosci. Model Dev.* **6**, 179-206, doi:10.5194/gmd-6-179-2013 (2013).

144 Lamarque, J. F. *et al.* Historical (1850–2000) gridded anthropogenic and biomass burning emissions of reactive gases and aerosols: methodology and application. *Atmos. Chem. Phys.* **10**, 7017-7039, doi:10.5194/acp-10-7017-2010 (2010).

145 Donner, L. J. & al., e. The Dynamical Core, Physical Parameterizations, and Basic Simulation Characteristics of the Atmospheric Component AM3 of the GFDL Global Coupled Model CM3. . *J. Climate* **24**, 3484–3519, doi:doi: http://dx.doi.org/10.1175/2011JCLI3955.1 (2011).

146 Wild, O., Zhu, X. & Prather, M. J. Fast-J: Accurate simulation of in- and below-cloud photolysis in tropospheric chemical models. *J. Atmos. Chem.*, **37**, 245-282 (2000).

147 Cionni, I. *et al.* Ozone database in support of CMIP5 simulations: results and corresponding radiative forcing. *Atmos. Chem. Phys.* **11**, 11267-11292, doi:10.5194/acp-11-11267-2011 (2011).

148 Li, D. & Shine, K. P. A 4-Dimensional Ozone Climatology for UGAMP Models, . (1995).

149 Dentener, F., van Weele, M., Krol, M., Houweling, S. & van Velthoven, P. Trends and inter-annual variability of methane emissions derived from 1979-1993 global CTM simulations. *Atmos Chem Phys* **3**, 73-88 (2003).

150 Huijnen, V. *et al.* The global chemistry transport model TM5: description and evaluation of the tropospheric chemistry version 3.0. *Geosci. Model Dev.* **3**, 445-473, doi:10.5194/gmd-3-445-2010 (2010).

151 Williams, J. E., Strunk, A., Huijnen, V. & van Weele, M. The application of the Modified Band Approach for the calculation of on-line photodissociation rate constants in TM5: implications for oxidative capacity. *Geosci. Model Dev.* **5**, 15-35, doi:10.5194/gmd-5-15-2012 (2012).

152 Naik, V. *et al.* Preindustrial to present-day changes in tropospheric hydroxyl radical and methane lifetime from the Atmospheric Chemistry and Climate Model Intercomparison Project (ACCMIP). *Atmos. Chem. Phys.* **13**, 5277-5298, doi:10.5194/acp-13-5277-2013 (2013).